1-1-2013

Geometric Optimization of Retroreflective Raised Pavement Markers

Lukai Guo
University of South Florida, lukai@mail.usf.edu

Geometric Optimization of Retroreflective Raised Pavement Markers

by

Lukai Guo

A thesis submitted in partial fulfillment
of the requirements for the degree of
Master of Science in Civil Engineering
Department of Civil and Environmental Engineering
College of Engineering
University of South Florida

Major Professor: Qing Lu, Ph.D.
Abdul R. Pinjari, Ph.D.
Manjriker Gunaratne, Ph.D.

Date of Approval:
March 20, 2013

Keywords: Orthogonal Design, Regression Model,
Von Mises Stress, Survey, Finite Element

DEDICATION

This thesis is dedicated to my father, Genlin Guo and my mother, Xiaoyan Lu for their endless love, patience, and understanding. I am eternally indebted to them for their generosity and encouragement through my life.

ACKNOWLEDGMENTS

Let me express my deepest gratitude to my advisor, Dr. Qing Lu, for his constant guidance and support throughout my master program. I thank him for his active encouragement, excellent inspiration and invaluable ideas that gave me the chance to learn and experience research. I also would like to thank Dr. Pinjari and Dr. Gunaratne for serving on my thesis committee. Special thanks to the teammate of my research group, Bin Yu, who assisted me tremendously in completing the research and testing.

TABLE OF CONTENTS

LIST OF TABLES

LIST OF FIGURES

ABSTRACT

As the field service life of retroreflective raised pavement marker (RRPM) is much shorter than expected, it is necessary to identify the causes and thus improve the RRPM structural design to mitigate the main failure modes, such as poor retention from pavements, structural damage, and loss of retroreflectivity. One strategy for extending RRPM service life is to enhance RRPM geometric characteristics to decrease critical stresses in markers. The main purpose of this thesis is to analyze the relationship between stresses, failure modes, and RRPM profiles. Based on this research, some measures are suggested in order to avoid corresponding failure modes by optimizing RRPM profiles.

The information about current performance of different types of RRPMs is summarized through literature review, questionnaire surveys, and a series of field surveys in Tampa bay area. Field survey observations show that the RRPM failure modes include lens cracking, lens loss, body cracking, body breakage, complete loss of RRPMs from pavement surface, severe abrasion or contamination of the retroreflective faces, and sinking of RRPMs into asphalt concrete. The overall performances of RRPMs in surveyed pavement sections are summarized and ranked as: 3M 290> Rayolite RS >Ennis 980>Ennis C80>Apex 921AR.

The distributions and magnitudes of various stress indicators, such as von Mises stress, principal stress, shear stress and normal stress within the RRPM structure, are estimated by finite element model (FEM) of pavement/tire/marker systems in ANSYS

software. Based on finite element model simulations, the critical stresses in the RRPMs and the observed failure modes are linked. Both the critical von Mises stress and compressive stress are concentrated on the rims and corners of the markers' top surface. Tensile stress is produced on the mid-top of markers' shell and distributed symmetrically. For shear stress at the RRPM bottom, the maximum one occurs on the non-lens sides of the RRPM. Upward normal stress, which may cause RRPM detachment from pavement, exists at the bottom, especially on the edge of lens side and at the middle of the curve edge.

One orthogonal experiment of a matrix of $L_{16}(4^{5-3})$ and one full factorial experiment of 4×5 were used to guide the FME simulations. Based on the stress magnitudes variations on different RRPM types, the relationships between the RRPM profiles and the stresses are obtained. It is found that RRPMs of geometric designs of smaller bottom width and top length, larger bottom length, lower height, and lower ratio of top width over bottom width witness decreases of experienced critical stresses.

CHAPTER 1: INTRODUCTION

1.1 Background

Retroreflective raised pavement marker (RRPM) is a device that is applied as a positioning guide to supplement or substitute for pavement markings (FHWA, 2003), especially during night and wet weather conditions when the pavement markings experience a substantial reduction of retroreflectivity. Moreover, RRPM can also cause vehicle vibration and audible tone to alert drivers for crossing over it (NCHRP, 2004).

However, the Texas Department of Transportation conducted a number of studies to conclude that most RRPMs lose reflectivity over very short periods of time (Hofmann and Dunning, 1995). In recent years, RRPMs exhibited poor field performance, such as poor retention on pavements, structural damage, and loss of retroreflectivity (Zhang et al., 2009).

These unexpected damages significantly reduce RRPM service life. Considering the relatively high cost of RRPM (material and installation), based on benefit-cost calculation, most states do not install RRPMs if pavement overlay or replacement is scheduled within five years or less (Matthias, 1988; Zador et al., 1982). This strategy also can be interpreted that the anticipated RRPM service life should be beyond five years, otherwise the negative profit appears. However, questionnaire survey, conducted by a University of South Florida (USF) investigation team, shows that the average RRPM

service life is 28.6 months, which is less than half of the expected minimum service life. Therefore, it is important to investigate how to extend the RRPM service life.

1.2 Organization of the Thesis

The thesis is organized as follows. As a preparation for the study, the remainder of Chapter 1 introduces all types of RRPMs, which were collected by searching all states Department of Transportation (DOT) specifications and attached Qualified Product Lists (QPLs). Chapter 2 shows the current performance of these RRPMs according to questionnaire and field surveys. The questionnaire survey was conducted with participants including maintenance engineers, contract managers, and other personnel in various state DOTs. The field surveys were conducted around the Tampa Bay area of Florida. Chapter 3 describes the methodology of building a finite element model (FEM) of the tire/marker/pavement system to simulate the RRPM conditions in the real world. Chapter 3 also describes the experimental designs, including one orthogonal design and one full factorial design. The rest of Chapter 3 introduces different critical stresses and why these types of stresses are considered. Chapter 4 is divided into three parts. The first part analyzes the magnitudes and locations of critical stresses on some typical size RRPMs. The second part conducts statistical analysis of stresses. The third part verifies the FEM simulation results based on the survey results in Chapter 2. Conclusions and future researches are listed in Chapter 5.

1.3 Types of RRPMs

RRPMs can be classified in various ways based on their structures and functions. According to a common classification used in Florida Department of Transportation (FDOT) 2010 Standard Specifications for Road and Bridge Construction, Section 970,

RRPMs in Florida are mainly grouped into four classes: Class A for temporary, Class B for permanent, Class D for work zone, and Class E for temporary work zone. Many other states further separate the permanent RRPMs into two subcategories: snowplowable and nonsnowplowable. Snowplowable RRPMs typically consist of cast iron housing and reflective lens, and are used in snowplow regions, like the northern states of the USA. Nonsnowplowable RRPMs do not have protective housing, and thus are only suited for roadways that do not experience snow plowing, such as those in Florida. Based on a comprehensive review of DOT specifications and qualified or approved product lists (QPLs/APLs) of RRPMs in each state, the use of snowplowable or nonsnowplowable RRPMs in the US is summarized in Figure 1-1.

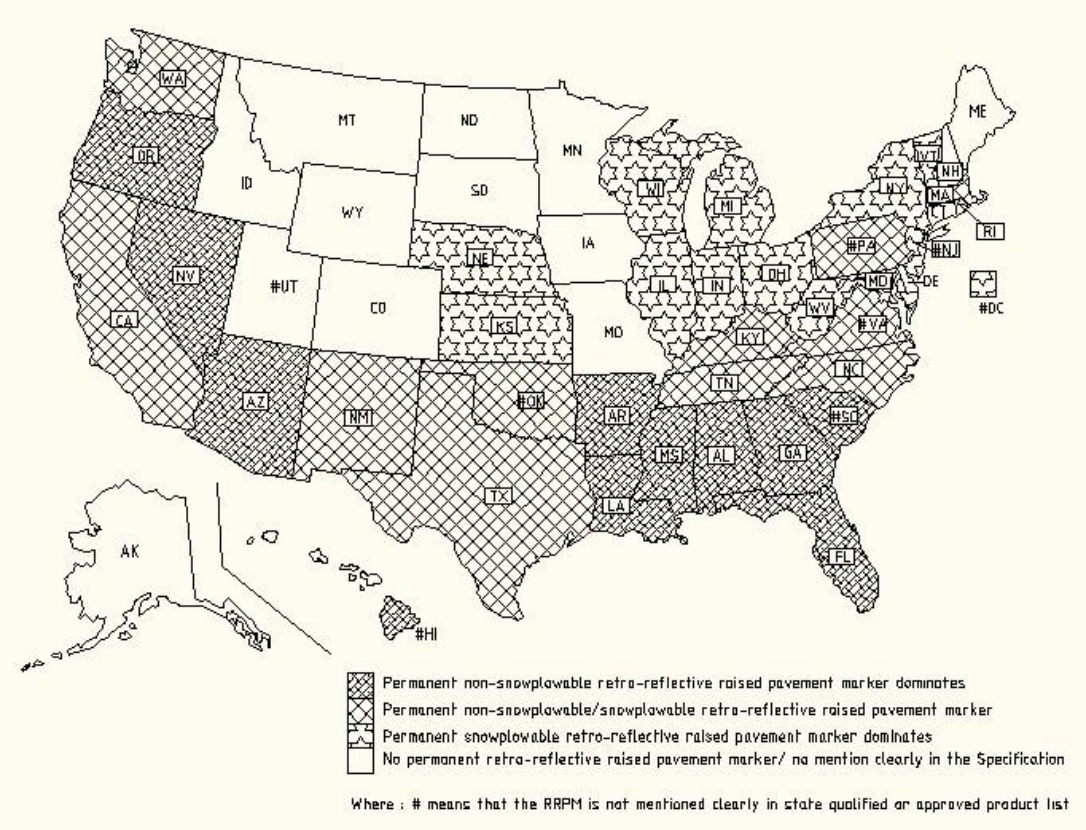

Figure 1-1 Use of Snowplowable or Nonsnowplowable RRPMs in the U.S.

Figure 1-1 shows that the states using permanent nonsnowplowable RRPMs are concentrated in the southern areas where air temperature is relatively high. This map also shows that, in many northern areas, permanent nonsnowplowable RRPMs are typically not installed.

Since this study is intended for the RRPM use in Florida of rare snow chances, only nonsnowplowable RRPMs are of interests. Figure 1-1 shows how widely this type of RRPMs is used. Because all information in this map was derived from DOT specifications and QPLs/APLs, the map only describes the current use of RRPMs on U.S. Route highways, U.S. Interstate highways, and State Route highways. The use of RRPMs on local roads and streets is not included. During the survey, it was discovered that a few states have recently stopped the use of nonsnowplowable RRPMs and begun to use snowplowable ones instead.

Based on the state DOT QPLs/APLs, four companies are mainly approved for providing nonsnowplowable RRPMs:

1) 3M

2) Ennis/Stimsonite

3) Ray-o-lite, and

4) Apex

For 3M, the major product is 290 series, including 290PSA series (PSA stands for pressure sensitive adhesive, which means a simple pressure can activate the adhesive function); For Ennis/Stimsonite, the company provides 6 widely used types of RRPMs: C80, C88, Model 911, Model 980, Model 948, and Model 953; For Apex, only 921AR is mentioned, but widely appearing, on the States QPL/APL; For Ray-o-lite, the AA (All

Acrylic), RS (Round Shoulder), SS (Squared Shoulder), and Model 2002 are the main products. The AA and RS types also include ARC (abrasion resistant coats) and FH categories. The use of these RRPMs in various states is summarized in Table 1-1, and plotted in Figure 1-2.

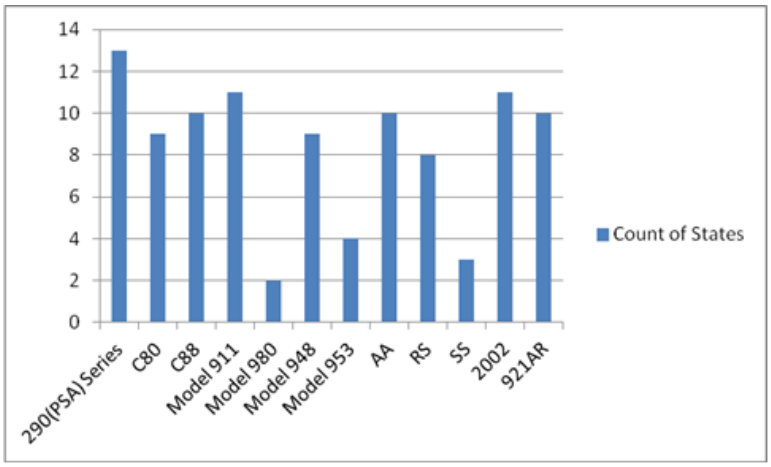

Figure 1-2 Number of States Using Various Models of RRPMs

Table 1-1 Current Types of RRPMs in the US States

	3M	Ennis/ Stimsonite						Ray-O-Lite				Apex
State	290(PSA)	C80	C88	911	980	948	953	AA	RS	SS	2002	921AR
Alabama	✓		✓			✓		✓	✓		✓	✓
Arizona	✓	✓	✓	✓	✓		✓	✓			✓	
Arkansas	✓			✓		✓						✓
California	✓		✓	✓		✓	✓	✓	✓	✓	✓	✓
Florida	✓	✓			✓				✓			✓
Georgia	yellow	✓		✓		✓			✓		✓	✓
Louisiana	yellow/blue	✓		✓		✓		✓	✓		✓	✓
Mississippi			✓	✓						✓	✓	
New Mexico	✓											
North Carolina		✓	✓					✓		✓	✓	
Tennessee	✓		✓	✓		✓		✓			✓	✓
Texas	✓	✓	✓	✓				✓	✓		✓	✓
Nevada	✓	✓	✓	✓			✓	✓	✓			✓
Oregon			✓	✓		✓		✓				
Washington	✓	✓	✓	✓		✓	✓	✓	✓		✓	✓
Massachusetts	✓	✓										
Kentucky						✓					✓	

According to their various materials and structures, RRPMs can be grouped as follows.

1.3.1 With or Without Fill Materials

Typical RRPMs without fill material are 3M 290 series and Ennis C80. The body structure is hollow as illustrated in Figure 1-3.

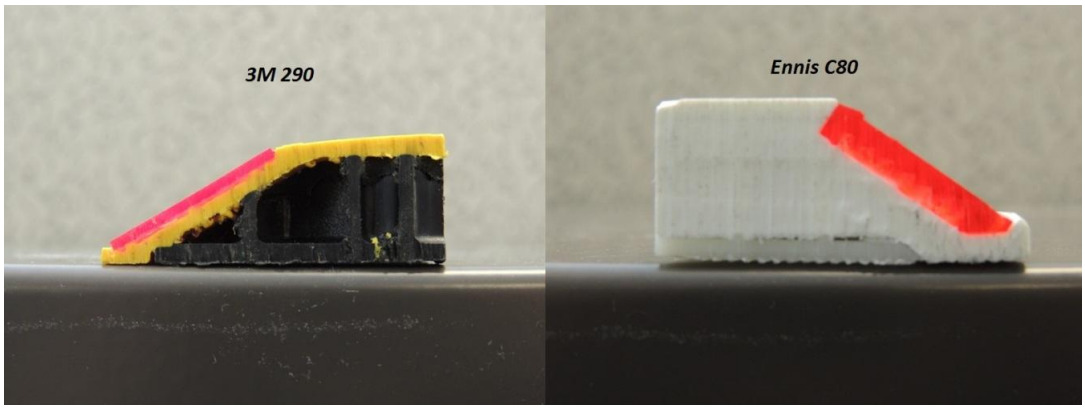

Figure 1-3 Cross Sections of 3M 290 and Ennis C80

RRPMs shown in Figure 1-4 are with filler material, such as Rayolite RS and Ennis C88.

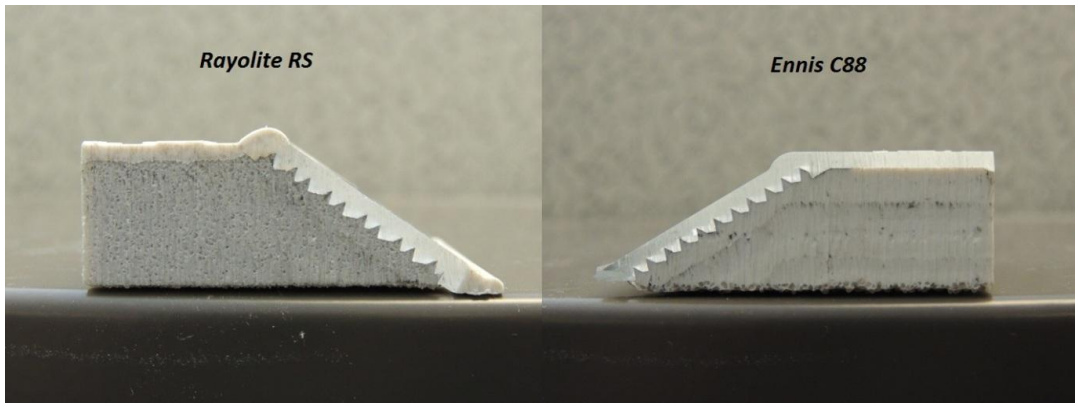

Figure 1-4 Cross Sections of Ennis C88 and Rayolite RS

1.3.2 Squared Bottom or Bottom With Curves

Geometrically, RRPMs can be divided into two categories: type I with squared bottom, such as Ennis C88, and type II with bottom with curve, such as Ennis C80.

For type I, the radius of bottom curve can be determined from bottom width and length directly, based on their relationship shown in Figure 3-2. These bottom curves also extend RRPM widths, and the width in this type is termed as extended width, which is shown in Figure 1-5. For type II, its squared bottom can be treated as one special case of type I, whose radius of curvature is infinite.

Moreover, different from type I, the bottom width of type II is unequal to its top width. However, this specific classification method is only for investigating the effects of change in RRPM geometric characteristics (outline of RRPM profile), without consideration of shell and filling material components.

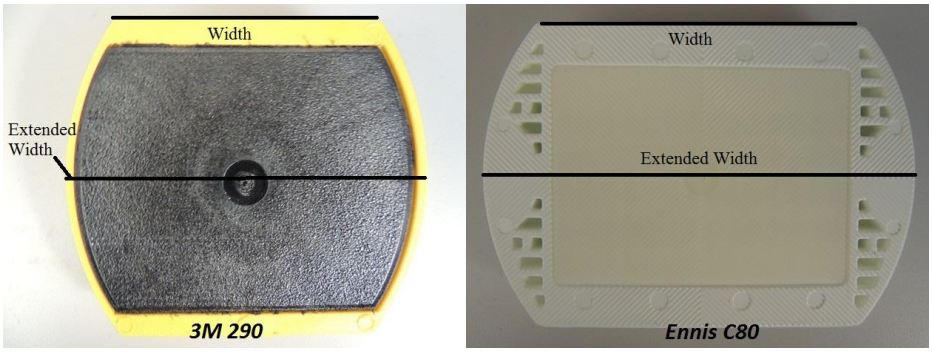

Figure 1-5 Bottoms of 3M 290 and Ennis C80

Because both types of RRPM profiles can be depicted by five variables (bottom length, bottom width, top length, top width and height), this classification is selected to be used in the subsequent study for geometric optimization.

Specifically, when building the FEM in ANSYS, changing the bottom shape can directly switch these two types of RRPM profile to each other. As a consequence, the geometric analysis of RRPM profiles can be concentrated on the marker which not only has bottom with curves, but also has unequal bottom width and top width.

Figure 1-6 Bottoms of Rayolite RS and Ennis C88

CHAPTER 2: QUESTIONNAIRE SURVEY AND FIELD SURVEY

2.1 Details of Questionnaire Survey

To collect up-to-date information on RRPMs from experienced engineers and specialists, a questionnaire survey was developed and distributed electronically across the nation. The respondents include maintenance engineers, contract managers, and other personnel in various state DOTs. Based on the relevancy to the purposes of the study, the respondents are divided into three groups: Group A from FDOT District 7 (Tampa area), Group B from other FDOT Districts, and Group C from other states (mainly DOT personnel with a few from the industry). The questions in the questionnaire vary slightly among the three groups. Among a total of 11 questions in the questionnaire survey, only two are directly related to geometric optimization. In this study, these two questions and corresponding responses are summarized, as follows, to provide useful information for further analysis.

Question 1 to Groups A, B, and C is what types of RRPMs (based on FDOT qualified product list if in Florida) are most commonly used? Why? Are there any RRPMs seen as good markers and any seen as bad markers in terms of field performance?

Response from Group A shows that 3M and Stimsonite are more commonly used due to pricing. 3M is seen as a good marker which has a longer life on the road and Stimsonite as not so good in the area of field performance. The markers shall comply

with ASTM D 4280 Class A (no abrasion treatment) and Class B (with abrasion treatment).

Response from Group B shows that Type B markers which are listed on the FDOT QPL are only used. The certification of materials is checked before beginning work. No significant difference in performance between manufacturers.

Response from Group C shows that Georgia uses 2×4 inches or 4×4 inches size RRPMs. All approved markers have similar service lives. In South Carolina, plastic makers with reflective surfaces, such as the 3M markers, have become more popular in recent years. Typically, Ray-O-Lite, Ennis (Stimsonite) and 3M markers which meet the general requirements of specifications are used on contracts. Louisiana uses 3M because of low bids. Contractors also seem to use more of the Ennis and Ray-O-lite markers. The Ennis markers seem to hold up better.

Arkansas uses 3M, Ennis, and Ray-O-Lite markers according to Supply Contract Specifications. No significant difference exists in performance between manufacturers. In Arizona, 3M 290 markers have dominated for quite a while. Ennis 88, 911 and 980, Apex 920 or 921, Ray-O-Lite round shoulder, ARC II markers have been approved, but are not often used. Washington State typically uses the Stimsonite model 88 RRPMs in Olympic Region because they last up to the plow abuse and normal highway use. Other RRPMs similar to the Stimsonite 948 ones are also used in Washington but they do not hold up well.

One respondent from California thinks that 3M is the best type: they seem to outlast all others by far as reflectivity is concerned. Respondents from Nevada and North Carolina only mentioned 3M but no significant difference exists.

Thus, 3M, Ennis, and Ray-O-Lite are the most popular RRPMs manufacturers in these states. 3M has dominated for quite a while because of its low bids and good performance. Apparently, the types of applied RRPMs vary with states, but the mainstream exists. Figure 2-1 shows that all these 7 states use 3M, and adversely, Apex is not so popular.

For field performance, Group A prefers 3M, and regards Stimsonite as not so good. Group B claims that there is no significant difference in performance between manufacturers.

In Group C, three respondents have the same comment as Group B. One respondent from Louisiana feels that Ennis seems to hold up better, and another respondent from Arizona replies that 3M dominates. Figure 2-2 shows that most of the respondents feel no significant difference in field performance of these approved RRPMs.

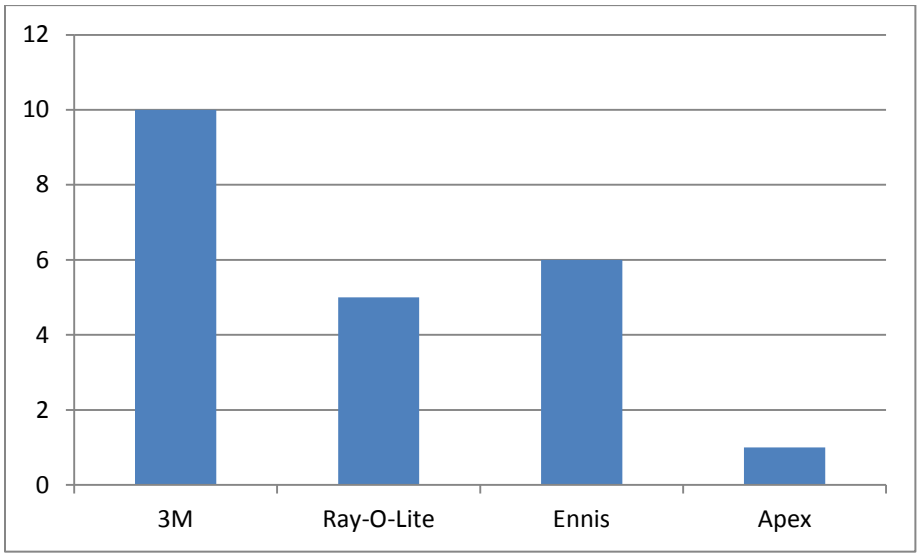

Figure 2-1 Numbers of States Using Various RRPMs

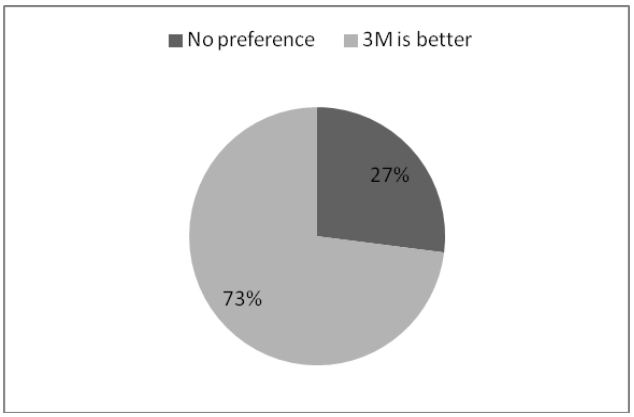

Figure 2-2 Comments and Their Percentages

Question 2 to Groups A, B, and C is what failure modes are often observed (e.g., lens cracking, RRPM body cracking, and loss of RRPMs [adhesive failure]) on asphalt pavements/ concrete pavements?

Response from Group A shows that, based on observed damage, it is true that most of the encountered damages are lens and body cracking, and scuffing of the lens surface. Moreover, there is one more item of failure modes: compression into the pavement surface, which typically occurs on new asphalt. The adhesion tracking onto lens caused by sun heating, rain and dirt is also treated as damage.

Response from Group B shows that, for the failure modes on asphalt pavements, the respondents' answers are different, as listed in Table 2-1 and plotted in Figure 2-3. As can be seen, lens and body cracking, sinking, and loss are the three main observed failure modes of RRPMs on asphalt pavements in Florida. Additionally, two respondents emphasized that the loss of RRPMs should be the most failure mode. For the failure modes on concrete pavements, the results are consistent: adhesive failure.

Table 2-1 Main Failure Modes and Number of Respondents in Group B

	Failure Modes		
	Loss	Crack	Sink
Number of Respondents	3	3	1

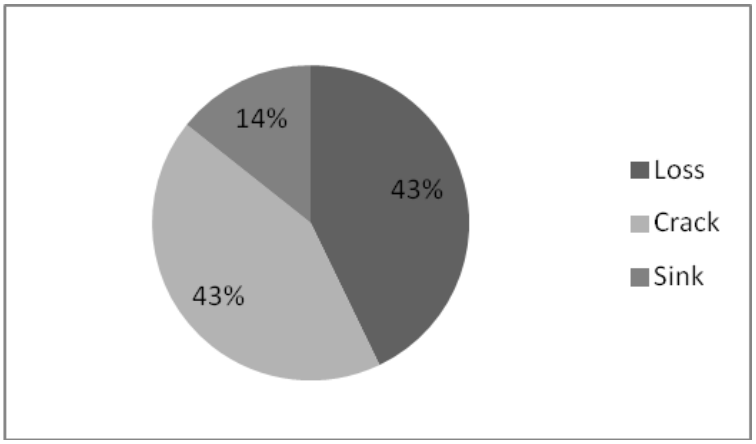

Figure 2-3 Main Failure Modes and Percentage of Respondents in Group B

Response from Group C shows that, for the failure modes on asphalt pavements, answers are similar to those from Group B. The specific results are shown in Table 2-2. For markers on concrete pavements, the failure modes are similar to those on asphalt pavements, with the exception of sinking.

Table 2-2 Main Failure Modes and Number of Respondents in Group C

	Failure Modes		
	Loss	Crack	Sink
Number of Respondents	7	7	3

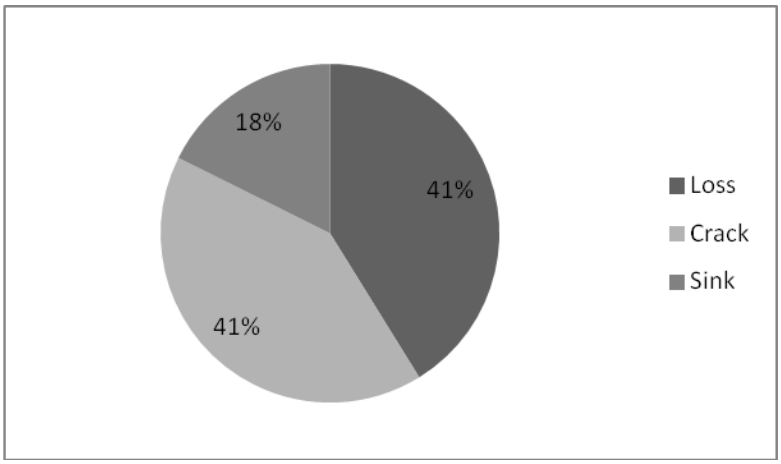

Figure 2-4 Main Failure Modes and Percentage of Respondents in Group C

Thus, based on the respondents' answers, it is safe to say that lens and body crack and loss of RRPMs are the main failure modes, and their proportions are almost equal.

This questionnaire survey also asked respondents for some suggestion, which can be done, to extend RRPM service life. There are two suggestions related to optimizing RRPM geometric characteristics. One is to decrease the RRPM profile height, and the other is to enlarge RRPM bottom area. These suggestions will be checked in Chapter 4.

This questionnaire survey also directly asked respondents in different states about whether their state uses RRPMs. Six respondents who respectively work in Virginia, Pennsylvania, Tennessee, New Mexico, Oklahoma, and Kentucky replied no, although their DOT specifications do mention RRPMs. Considering the weather conditions, these DOTs all use snowplowable RRPMs and temporary RRPMs, instead. Their answers contribute to modifying the "RRPM map", which is shown in Figure 2-5.

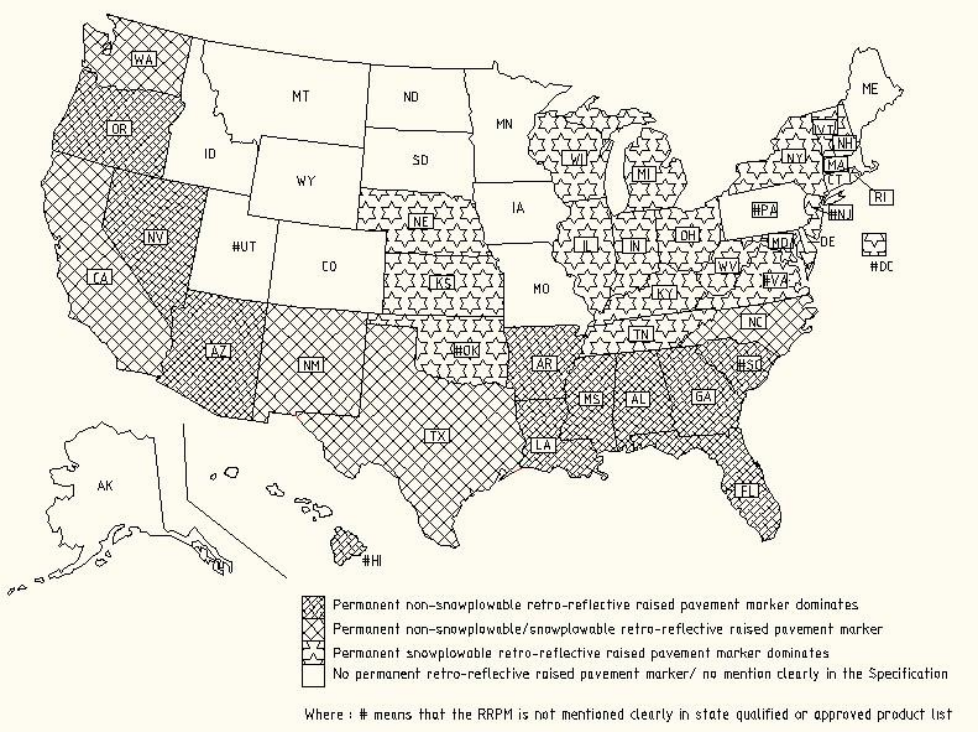

Figure 2-5 Modified Map of Use of Snowplowable or Nonsnowplowable RRPMs in the US

2.2 Details of Field Survey

In the summer and the fall of 2012, two field surveys with several objectives were conducted to record the conditions of RRPMs installed on selected FDOT roadways. Considering optimization of RRPM geometric characteristics, only the following two parts are discussed in this study:

1) Which types of RRPMs are widely used on FDOT roadways and how do they perform?

2) Which major failure modes do the RRPMs exhibit in the field?

2.2.1 Site Selection

The roadway sections surveyed, as shown in Figure 2-6, were selected through consulting with FDOT personnel to cover various marker types and damage conditions and high and low traffic volumes. One route, starting 10 miles south of Ruskin, along US 41, and then turning to SR 674, till the intersection with Plant City-Picnic Rd. The second route is along the Dale Mabry Hwy and 22 St, which are connected by SR 60. The third route is along 22 St, crossing SR 60, to the Causeway Blvd, until the intersection with Maydell Dr. These sections have various geometric features, such as tangent, horizontal curve, vertical curve, width and position (entry and departure approaches at intersections). The current traffic conditions, such as annual average daily traffic (AADT), truck volume, pavement surface condition (e.g., cracking and roughness) are also different.

The geometric characteristics and the conditions of the roadways were determined from the geographic information system (GIS) data and Straight Line Diagrams (SLDs), which are both available on FDOT website. The RRPMs and their failure modes were recorded by a digital camera.

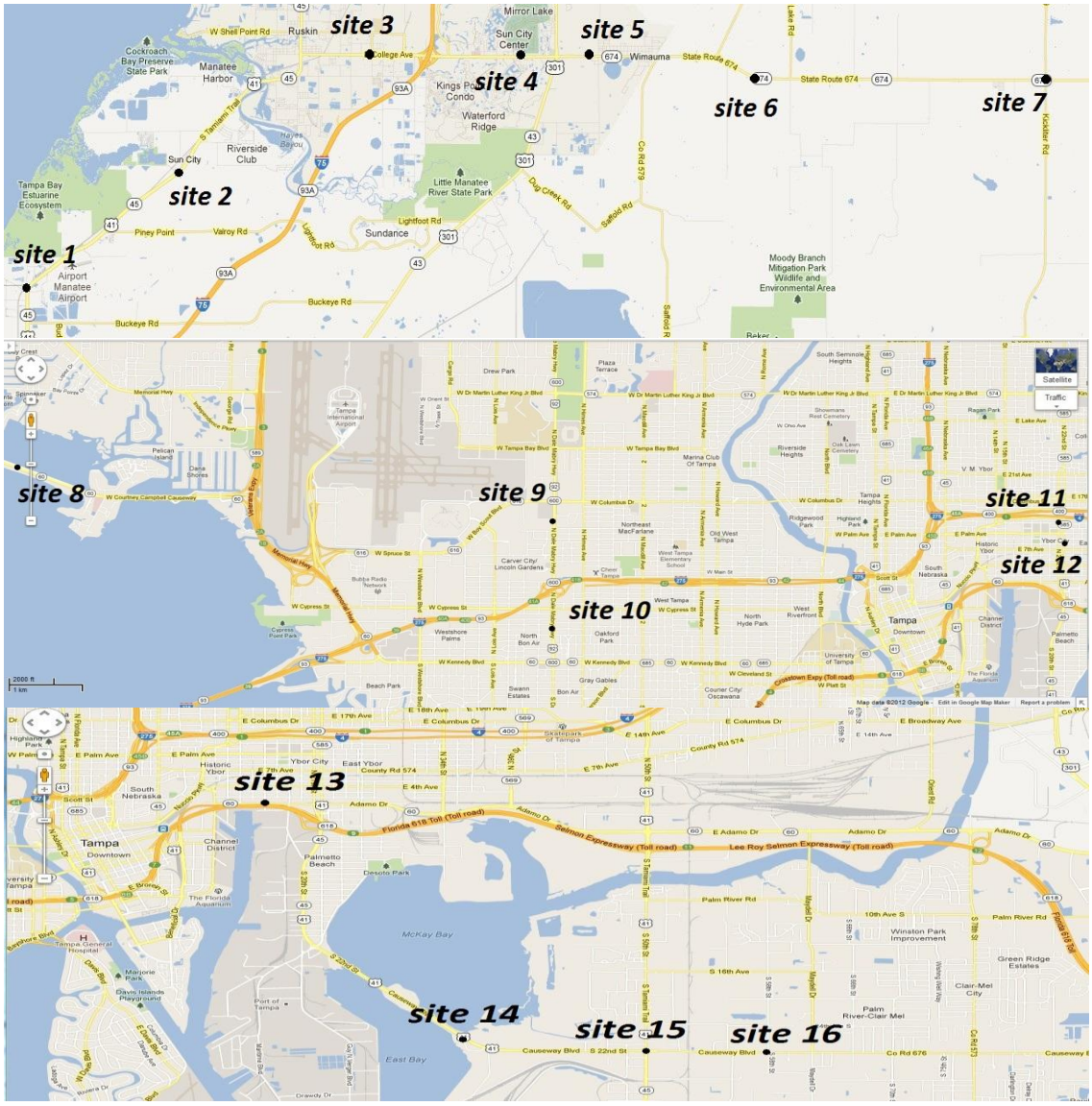

Figure 2-6 Locations of Roadway Sections Surveyed

2.2.2 Field Survey in May, 2012

The major failure modes on different RRPM types were observed during the field survey in May, 2012.

Generally, the RRPM failure modes can be identified into four types: lens breakage and loss; cracking of the RRPM body; complete loss of RRPM from pavement surface; and severe abrasion or contamination of the retro-reflective faces (Zhang et al., 2009). For more accurate description, this study further separates the specific modes into

seven categories, as follows:

1) LC: lens cracking

2) LL: lens loss

3) BC: body cracking

4) BB: body breakage

5) LR: complete loss of RRPMs from pavement surface with only adhesive remaining

6) AC: severe abrasion or contamination of the retroreflective faces

7) S: sinking of RRPMs into asphalt concrete

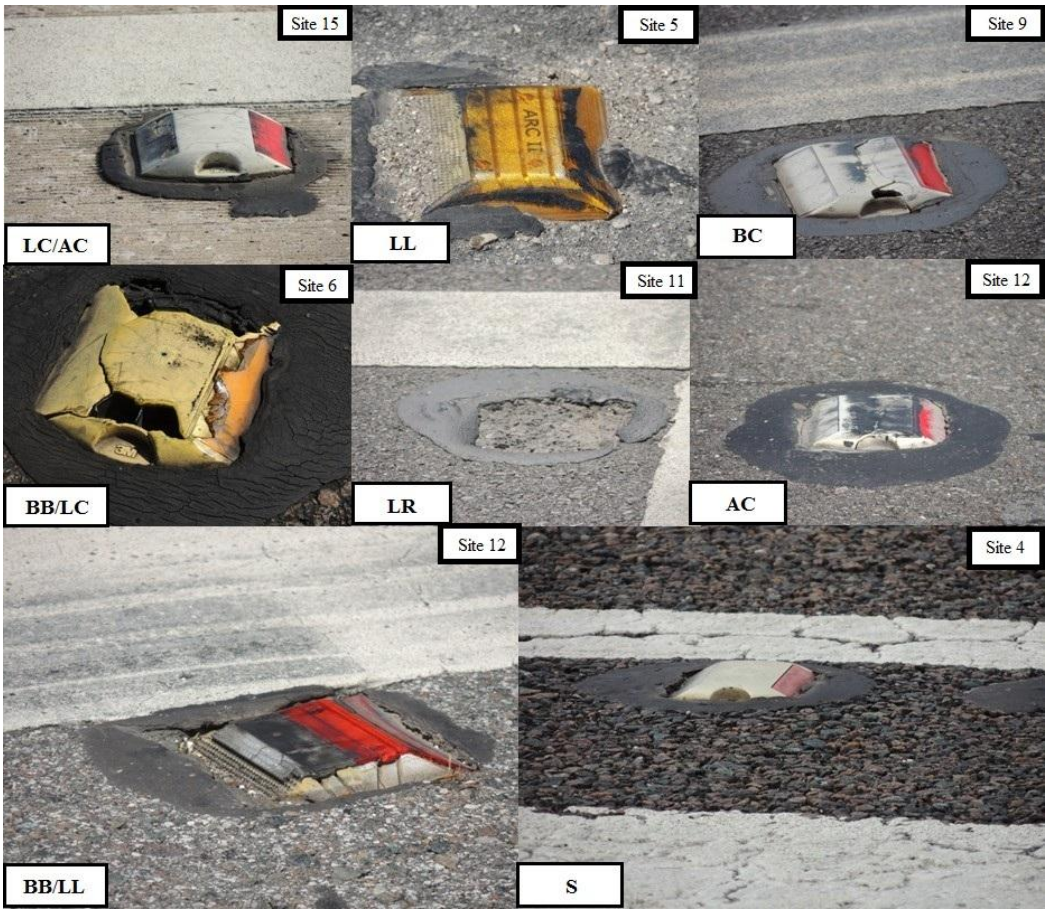

Figure 2-7 Failure Modes

Based on the condition survey on the selected FDOT roadways, the counts of sites where different failure modes were observed are shown in Table 2-3.

Table 2-3 Counts of Sites with Different Failure Modes of Four RRPM Brands

	LC	LL	BC	BB	LR	AC	S	No. of Sites Surveyed
3M 290	1	0	2	2	3	10	6	11
AA ARC II	3	2	3	1	2	3	1	5
C80	0	0	0	0	0	1	0	1
Round Shoulder	0	0	0	0	0	1	0	1

It can be seen from Table 2-3 that:

1) 3M 290 is most widely used at these field survey sites, followed by AA ARC II.

2) For 3M 290 markers, their lenses are relatively sturdy, because no lens loss (LL) was observed at these sites. However, frequent abrasion or contamination of the lens surface (AC) and marker sinking (S) were observed.

3) AA ARC II exhibited various distress modes without any single mode dominating.

4) The marker bodies of 3M 290 and AA ARC II all seem to be weak in the middle. It is observed that the middle body of 3M 290 has to bear more loads, because of its finger grips. AA ARC II has an abrasion resistant coating which is separated into two bond parts. The bond boundary in the middle body of the RRPMs seems to be a weak layer for cracking.

5) C80 and Round Shoulder markers only show abrasion or contamination of the retroreflective faces. They were only observed on portland Cement Concrete (PCC) pavements in this survey. Compared with 3M 290, C80 may protect the lens more effectively since its lens is slightly dented.

6) Many RRPMs' failure extents are not commensurate with the roads' condition,

such as those at sites 1, 2, 4, 5, 8, 9, 10, 13, 14, and 15. These sites sustained heavy truck traffic and showed pavement distresses such as cracking, but the markers looked fine. One potential reason is that the markers had been replaced frequently. One example is at site 13 (on SR 60), where the remaining adhesives on the pavement indicated that the markers had been replaced for at least four times in the last few years. The age information of the markers, however, could not be obtained from FDOT, which limited the extent of analysis of the field data and made ensuing field surveys indispensable.

For better evaluation of the current RRPM situations, the method to measure the performance of RRPMs are in accordance with NTPEP (National Transportation Product Evaluation Program):

$$R = \sum_{i=0}^{5} \beta_i R(i)$$

where:

R = Total Rating,

R (i) = Rating defined by NTPEP,

R (5) = 5-Excellent; Completely Intact, “Like New” Condition,

R (4) = 4-Good; Minor Scrapes and Scratches,

R (3) = 3-Fair; Obvious Damage but still Functional,

R (2) = 2-Poor; Major Damage, Marginally Functional,

R (1) = 1-Very Poor; Non-functional,

R (0) = 0-Missing,

β_i = Estimated Proportion.

According to the estimated proportion of different RRPM ratings at different sites, as shown in Table 2-4, the total rating can be calculated from the equation above.

Table 2-4 RRPM Rating at Each Site from First Survey

Site ID	Marker Type	Survey 1							
			Performance						
		Date	1	2	3	4	5	0	Total
4	3M 290	5/10/2012				95%	5%		4.05
5	Rayolite AA ARC II	5/10/2012				95%	5%		4.05
6	3M 290	5/10/2012		10%	80%	10%			3
7	Rayolite AA ARC II (FH)	5/10/2012			15%	65%		20%	3.05
8	3M 290	5/11/2012				90%	10%		4.1
9	Rayolite Round Shoulder	5/11/2012				90%	10%		4.1
10	Ennis Paint Model C80	5/11/2012				70%	10%	20%	3.3
11	Rayolite AA ARC II (FH)	5/11/2012			70%	30%			3.3
12	3M 290	5/11/2012			50%	30%		20%	2.7
13	3M 290; Rayolite AA ARC II	5/21/2012				20%	80%		4.8
15	3M 290	5/21/2012			60%	20%		20%	2.6
16	3M 290	5/21/2012				50%	30%	20%	3.5

The total ratings for each RRPM type in Table 2-4 are averaged and shown in Table 2-5.

Table 2-5 Average Ratings of Various RRPM Types from First Survey

Marker Type	Average Rating
3M 290	3.53
Rayolite AA ARC II	3.8
Rayolite Round Shoulder	4.1
Ennis Paint Model C80	3.3

Table 2-5 shows that the Rayolite Round Shoulder has the best performance rank, and the other three RRPM types are all on "good-fair" level, based on the information from the field survey in May, 2012.

2.2.3 Field Survey in September, 2012

To clear the confounding effect of various RRPM ages, one ensuing field evaluation after four months was made to check whether the failure of RRPMs was exacerbated in the same time period for all sections.

Unfortunately, at sites 6, 7 and 8, the roads had been repaved and old RRPMs had been replaced. Therefore the RRPMs at these three sites cannot be considered for comparison with the RRPM former condition.

Similar to the first field survey, the total ratings of different RRPM types are calculated and shown in Table 2-6.

Table 2-6 RRPM Rating at Each Site from Second Survey

Site ID	Marker Type	Survey 2							
			Performance						
		Date	1	2	3	4	5	0	Total
4	3M 290	9/11/2012			5%	95%			3.95
5	Rayolite AA ARC II	9/11/2012				85%	5%	10%	3.65
6	3M 290	9/11/2012				20%	80%		4.8
7	Rayolite AA ARC II (FH)	9/11/2012				10%	70%	20%	3.9
8	3M 290	9/12/2012				5%	95%		4.95
9	Rayolite Round Shoulder	9/12/2012				90%	10%		4.1
10	Ennis Paint Model C80	9/12/2012				65%	10%	25%	3.1
11	Rayolite AA ARC II (FH)	9/12/2012			70%	30%			3.3
12	3M 290	9/12/2012			50%	30%		20%	2.7
13	3M 290; Rayolite AA ARC II	9/12/2012				20%	80%		4.8
15	3M 290	9/12/2012			40%			60%	1.2
16	3M 290	9/12/2012			20%	40%		40%	2.2

The total rating for each RRPM type in Table 2-6 are averaged and shown in Table 2-7.

Table 2-7 Average Ratings of Various RRPM Types from Second Survey

Marker Type	Average Rating
3M 290	3.51
Rayolite AA ARC II	3.9
Rayolite Round Shoulder	4.1
Ennis Paint Model C80	3.1

The average ratings of RRPMs obtained from the two field surveys are compared and shown in Table 2-8. RRPMs at sites 6, 7, and 8 are excluded in the comparison since they had been replaced.

Table 2-8 shows that 3M 290 got damaged more than the other three RRPM types. The failure of Rayolite AA ARC II and Ennis Paint Model C80 was slightly exacerbated, and the condition of Rayolite Round Shoulder seems to exhibit no change during these four months.

Table 2-8 Comparison of Average Ratings of Various RRPM Types from First and Second Surveys

Marker Type	Average Rating from 1st Survey	Average Rating from 2nd Survey
3M 290	3.53	2.97
Rayolite AA ARC II	4.05	3.9
Rayolite Round Shoulder	4.1	4.1
Ennis Paint Model C80	3.3	3.1

2.3 Summary of Current RRPM Conditions by Surveys

Evaluations of RRPMs from different sources, such as questionnaire survey, field survey, and literature review have already been obtained. However, every source has its own blind side. For example, a short-term field survey cannot fully show the different qualities of RRPMs, because of the capricious external conditions. Therefore, the task of this section is to summarize these evaluations individually, and then to combine them to get a comprehensive rank of those RRPMs that are used in Florida.

2.3.1 Questionnaire Survey

This survey directly provides general evaluations of different RRPMs from experienced engineers and specialists. The results show that 27 percent respondents select 3M 290 as the best type, and the rests have no significant preference. Thus, this questionnaire survey identifies 3M 290 as better performing than the other types of RRPMs.

2.3.2 Field Survey

In contrast with the questionnaire survey, field survey provides more details of RRPM performance. According to rating performances of RRPMs from two field surveys, which are shown in Table 2-8, the rank of RRPMs is determined as follows: Rayolite RS > Rayolite AA ARC II >Ennis C80-FH > 3M 290.

Specifically, the typical failure modes in different types of RRPMs are observed and shown in Figure 2-8. For Ennis C80, there is almost no damage on the body and lens. For Rayolite RS, severe abrasion occurs on the rim of body. For 3M 290, all failure types can be observed in different sites, such as lens cracking and loss, body cracking and breakage, completely loss, severe abrasion, and sinking into the pavement.

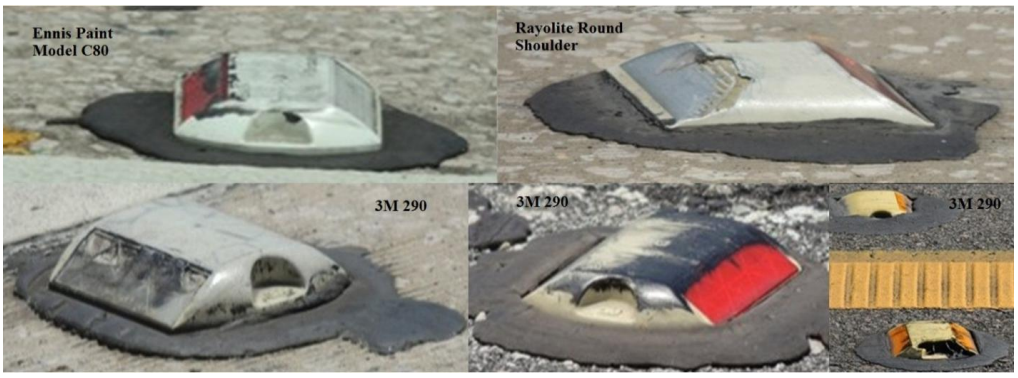

Figure 2-8 Typical Failure Modes in Different Types of RRPMs

2.3.3 Manufacturers' Information

Manufacturers also provide some related information about their products. However, to avoid bias, this part only compares two RRPMs manufactured from the same company. In Florida, only Ennis' two different RRPM modes are approved in the QPL. Ennis states that Ennis 980 marker is a new product which has higher performance and durability than their former products. It seems that Ennis 980 is the next generation of Ennis C80. Therefore, it is safe to say that Ennis 980 is more advanced than Ennis C80.

2.3.4 NTPEP Field Evaluation

NTPEP conducted field evaluations of RRPMs twice on Georgia test decks, respectively starting from 2004 and 2007. Ennis C80 and Rayolite RS were selected for the field evaluation in 2004 (NTPEP, 2004). Ennis 980 and Ennis C80 were installed for ensuing field evaluation in 2007 (NTPEP, 2011). Based on the raw records on the marker ratings, the average rating of every RRPM type can be calculated, and the results are shown as follows.

Table 2-9 RRPM Field Evaluation in Georgia

2004,Georgia				2007,Georgia			
		Ennis C80	Rayolite RS			Ennis C80	Ennis 980
6 Month	Concrete	3.842	3.963	6 Month	Concrete	3.675	3.531
	Asphalt	3.988	3.933		Asphalt	3.356	3.5
12 Month	Concrete	3.213	3.264	12 Month	Concrete	3.556	3.486
	Asphalt	3.042	3.139		Asphalt	2.785	2.826
18 Month	Concrete	2.859	2.979	18 Month	Concrete	3.523	3.469
	Asphalt	2.63	2.786		Asphalt	2.102	1.922
24 Month	Concrete	2.327	2.601	24 Month	Concrete	3.134	3.286
	Asphalt	2.464	2.47		Asphalt	/	/

Table 2-9 illustrates that Rayolite RS is better than Ennis C80, and the general performances of Ennis C80 and Ennis 980 are similar.

2.3.5 Other Literature Review

One two-year field test, which was conducted on test decks in Texas, shows that 3M 290 is better than Ennis C80 (Zhang et al., 2009), and Apex 921AR has a worse performance (Zhang et al., 2009).

Table 2-10 Results of RRPM Performance Ranking by Difference Sources

	No.	Results (rank)	Blind side of source	Reliability of source
Questionnaire survey	1	3M 290 is the best performing	No details of analysis / Only based on experience	Experience
Field survey	2	Rayolite RS > Rayolite AA ARC II >Ennis C80-FH > 3M 290	No control of various external conditions (e.g., age, truck volume)/Insufficient sites	Practical performance
Manufactures' information	3	Ennis 980>Ennis C80	No comparison between RRPMs from two different companies	Comparison between RRPMs from same company is reliable
NTPEP field evaluation	4	Rayolite RS>Ennis 980/Ennis C80	/	Sufficient samples/ Control of external conditions/ Practical performance/ Long time period
Other field test	5	3M 290>Ennis C80>Apex 921AR	/	Sufficient samples/ Control of external conditions/ Practical performance/ Long time period

Table 2-10 lists the results from different sources, with their blind sides and their reliabilities. Although each source provides different RRPM ratings, Table 2-10 shows that sources 1, 3, 4, and 5 are not conflicting. The performance of these RRPMs can be ranked as follows: 3M 290> Rayolite RS >Ennis 980>Ennis C80>Apex 921AR. However, source 2 conflicts with this sequence. Weighing the pros and cons, because of

their severe blind sides which are listed in Table 2-10, the ranking from source 2 is ignored. The result of source 2 also illustrates that the RRPM performance significantly depends on the external conditions.

As the final consequence, the estimated rank of RRPMs in Florida can be expressed as: 3M 290> Rayolite RS >Ennis 980>Ennis C80>Apex 921AR.

CHAPTER 3: METHODOLOGY

3.1 Finite Element Model of Tire/Marker/Pavement Systems

In the real world, RRPM is installed on flexible or rigid pavement and impacted by tires with different velocities, directions, and impact locations. This whole contacting process is not static, but dynamic. Moreover, RRPM and tire both have complex profiles which cannot be deemed as simple geometric objects. As a consequence, building finite element models (FEM) for this system can not only simulate and analyze the real stress-strain condition efficiently, but also modify the RRPM dimensions for obtaining optimal shapes conveniently and efficiently. This system can be separated into three components: pavement model, RRPM model, and tire model, as shown in Figure 3-1.

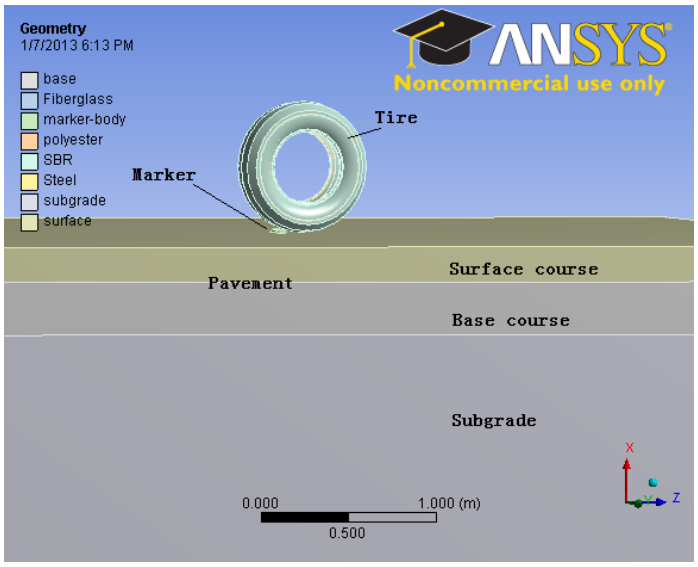

Figure 3-1 Tire/Marker/Pavement System

3.1.1 Pavement Model

Normally, pavement has two categories: flexible and rigid. For flexible one, it typically consists of three layers: surface of asphalt, base and subgrade courses of aggregates and soil. For rigid one, the surface is portland cement concrete instead and may be without base course. Because questionnaire and field surveys involve mainly flexible pavements in Florida, only flexible one is considered in this study. The following characteristics of a pavement model is obtained by Texas Transportation Institute (TTI) researchers and used in this study (Zhang et al., 2009). This pavement model matches the geometric designs of interstate highways bearing a large percentage of heavy traffic volume.

Table 3-1 Profiles and Material Properties for Flexible Pavement

Layer name	Thickness (m)	Density (kg/m^3)	Poisson's Ratio	Young's Modulus (MPa)
Surface	0.2	2322	0.35	3000
Base	0.3	2162	0.35	300
Subgrade	5.0	2001	0.35	10

3.1.2 Tire Model

Tire model, used in this paper, was previously developed by a USF investigation team for studying Locked Wheel Skid Tester (LWST) (Kosgolla, 2012). The cross sectional profile of this tire model is derived by slicing a spent standard ASTM E524-08 tire. This tire model consists of two fiberglass belted plies, two polymer biased plies, steel beads and tire rubber. As the main tire component contributing to friction, a tire rubber with styrene butadiene rubber (SBR) has both hyperelastic and viscoelastic properties. In ANSYS 12.0, Mooney-Revlin model can be developed for hyperelastic

property, and Prony series model can be applied for viscoelastic property. These relevant material properties and empirical constants are achieved from previous ASTM studies (ASTM 2001; ASTM 2006). Based on the above information, a three-dimension tire model is constructed in SolidWorks 2010 software, and then imported to the ANSYS platform for providing dynamic impact to RRPM.

3.1.3 RRPM Model

3.1.3.1 Details of RRPM Geometric Characteristics

As mentioned in Chapter 1, RRPMs can be divided into two categories: one with squared bottom, such as Ennis C88, and the other with curved bottom, such as Ennis C80. For Ennis C80, the radius of bottom curve can be plotted from bottom width and length directly, which is shown in Figure 3-2. In other words, the bottom curve is not an independent variable. As a consequence, without considering less significant geometric features, such as finger-grip, fillet, or chamfer, both types of RRPM model can be built by five basic factors: bottom width, bottom length, top width, top length and height.

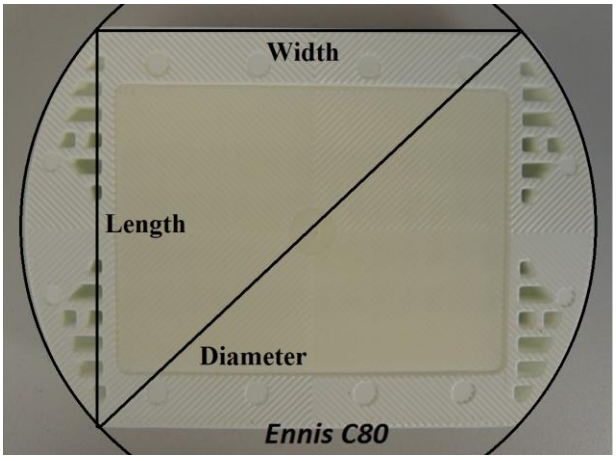

Figure 3-2 Geometric Relations on Bottom of Ennis C80

For more clearly describing the results obtained from ANSYS in the next chapter, Figure 3-3 defines and identifies all different parts of RRPM.

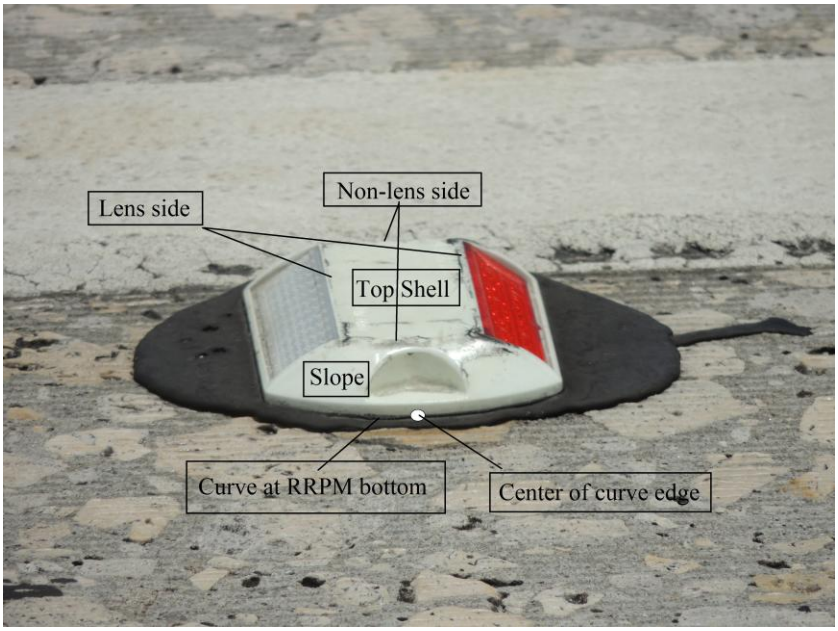

Figure 3-3 Different Parts of RRPM

3.1.3.2 Measurements of RRPMs and Material Properties

For dimensions of RRPMs, the precise geometry information was obtained by measuring the cut-into-piece substructure of the RRPMs with a vernier caliper. A list of the major geometry data of the four RRPMs is provided in Table 3-2. For material properties, an extensive literature review of multiple sources, such as manufacturer specifications, published studies, and Google searching, were performed to obtain the relevant material properties, which are summarized in Table 3-3 through Table 3-5.

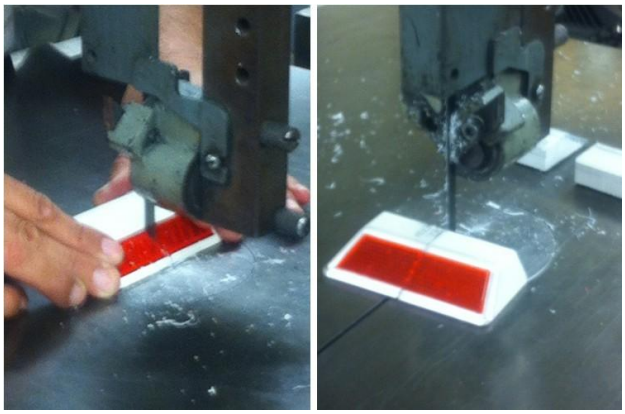

Figure 3-4 Cutting the RRPMs to Measure the Geometric Information

Table 3-2 Profiles of Each RRPMs (mm)

Type	Thickness	Length	Width	Top Length	Top Width
3M 290	15.7	88.9	72.3	44.9	69.8
Ennis C80	17.5	80.8	86.3	39.2	78.0
Ennis C88	18.1	101.0	101.0	40.1	85.8
Rayolite RS	17.3	99.3	100.2	48.8	57.5

Table 3-3 Material Properties of 3M 290

Body and Lens (Acrylic)		
Density	1350	kg/m^3
Young's modulus	5800	MPa
Poisson ratio	0.35	-
Yield strength	80	MPa

Table 3-4 Material Properties of Ennis C80

Body (Acrylic)		
Density	1040	kg/m^3
Young's modulus	2100	MPa
Poisson ratio	0.35	-
Yield strength	44	MPa
Lens (Acrylic)		
Density	1190	kg/m^3
Young's modulus	3103	MPa
Poisson ratio	0.11	-
Yield strength	70	MPa

Table 3-5 Material Properties of Rayolite RS

Filler (Inert Thermosetting Compound)		
Density		kg/m^3
Young's modulus	2600	MPa
Poisson ratio	0.44	-
Yield strength		MPa
Housing (Acrylonitrile Butadiene Stryrene)		
Density		kg/m^3
Young's modulus	2300	MPa
Poisson ratio	0.37	-
Yield strength		MPa
Lens (Methyl Methcrylate)		
Density		kg/m^3
Young's modulus	2450	MPa
Poisson ratio	0.37	-
Yield strength		MPa

3.1.3.3 Building RRPM Models in ANSYS

Two types of RRPMs are built in ANSYS based on the dimensions of RRPMs. And the material properties of each RRPM component are inputted into "Engineering Data" section in the software. In this study, as mentioned in section 1.3.2, the shape of RRPM is the combination of both types, which not only has bottom with curves, but also has unequal bottom width and top width.

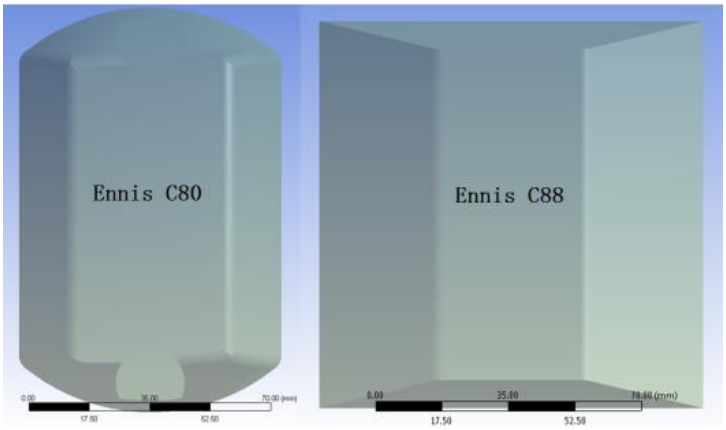

Figure 3-5 RRPM Model in ANSYS

3.1.4 Contact Model

Contact behavior is a highly nonlinear process, requiring special skills to assure the simulation accuracy. ANSYS provides powerful analysis tool to execute the contact command. In this study, surface to surface contact elements were used since they are suitable to detect the gap between the two contact interfaces. The pavement and maker are much stiffer compared to the rolling tire. Considering this, the pavement surface elements and the RRPM surface elements were treated as target elements (blue part in Figure 3-6) and the bottom surface elements of the rubber block were treated as contact elements (red part in Figure 3-6).

In this study, CONTA 174 element was selected as contact element since it is capable of changing the coefficient of friction with "temperature, time, normal pressure, sliding distance, or sliding relative velocity" (ANSYS, 2009). On the other hand, TARGE 170 was used as the target elements. Augmented-Lagrangian algorithm was used as the contact algorithm, which was able to prevent element penetration effectively (ANSYS, 2009). The stiffness matrix was updated for each iteration to obtain more accurate simulations at the expense of additional running time. The coefficient of friction (μ) was

defined using the Coulomb friction model and in the modeling, field surveyed value was used (ANSYS, 2009).

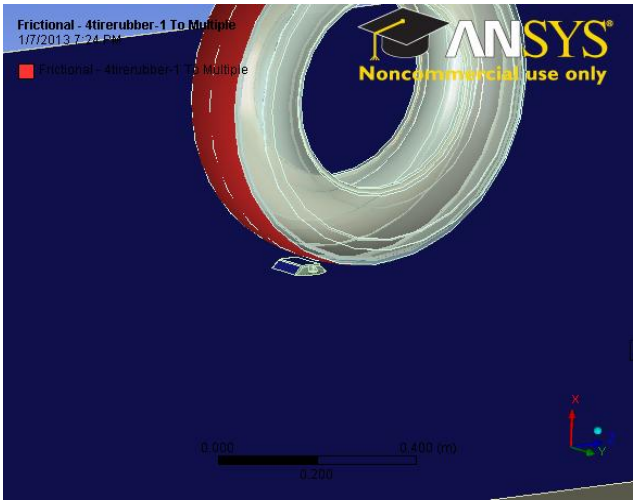

Figure 3-6 Tire-Marker Contact System

3.1.5 Mesh Generation

After building the tire-marker-pavement system and defining the contact model, this system can be directly meshed by "mesh" order in ANSYS. Because of this powerful function for generating mesh, the time-consuming issue from re-mesh whenever the RRPM dimensions are changed is avoided.

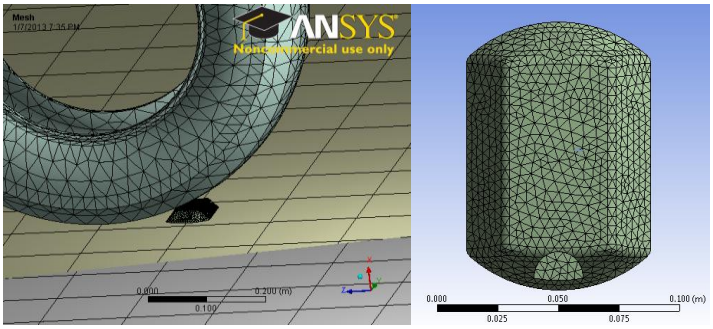

Figure 3-7 Mesh Generation

Because the sizes of tire, marker, and pavement are different, the finite element sizes are also defined by different values. Element sizes of tire, marker, and pavement are 4 mm, 40 mm, and 150 mm, respectively. Mesh generation also includes edge sizing:

eight edges of two pavement layers are selected and every edge is divided by three divisions.

3.1.6 Finite Element Model Assembly

In this part, the tire is molded to roll over the RRPMs dynamically. Several external factors, such as tire loading and vehicle velocity, are defined. Because the federal government limits vehicle weights and speeds on most interstate highways, these critical values are used in this study to define the tire load and vehicle velocity, which are 22200 N and 31.3m/s, respectively (Zhang et al., 2009). The boundary condition is that the bottom of sub-grade layer is set as "fixed support" for this system. After defining these external factors and assembling all the components, the whole system is simulated in ANSYS.

3.2 Experimental Design

After the completion of the previous work, the researcher continued to examine the effects of geometric factors—bottom length (BL), top length(TL), bottom width (BW), top width (TW) and height (H)—on the various stresses inside the markers, such as von Mises stress, principal stress, shear stress, and normal stress. The reasons of analyzing these stresses are specifically described in section 3.3. The levels of involved factors (BL, TL, BW, TW/BW, and H) are listed in Table 3-6.

Table 3-6 Matrix of Test Scenarios

Level	Element				
	BL (mm)	TL (mm)	BW (mm)	TW/BW	H (mm)
Lv. 1	80.2	40.1	64.3	0.85	14
Lv. 2	85.3	42.2	70.5	0.9	15.7
Lv. 3	90	44.6	75.2	0.94	17.5
Lv. 4	95	47.1	80.2	1	19.25

It is realized that the entire modeling program would involve $4^5 = 1024$ combinations of the levels of influencing factors, as shown in Table 3-6, for a full factorial design. Considering that every simulation takes at least two and a half hours using ANSYS, conducting all these tests is very much time consuming. To reduce the simulation work and meanwhile maintain the reliability of conclusions, an orthogonal design was used.

3.2.1 Orthogonal Design

3.2.1.1 Basic Concept of Orthogonal Design

Orthogonal design (Taguchi method) is a highly fractionated factorial design. This multi-factor multi-level experimental design selects some representative points from full-scale test to efficiently observe relationships between factors and effects. Because the selected points are evenly dispersed and neatly comparable, all interactions between the controls can be negligible.

Specifically, one typical example of fractional factorial design about four factors at three levels is introduced in detail as following.

If one experimental design has 4 factors and each factor has 3 levels, a full factorial design needs $3^4 = 81$ tests, as shown in Figure 3-8. Compared to the full factorial design, a fractional factorial design only needs $3^{4-2} = 9$ tests, as shown in Figure 3-9. Although the fractional factorial design omits many tests, it still can express the integral situation by highly representative tests. These selected tests are distributed evenly, without any redundancy.

Through fractional factorial design, because of uniform appearance of other control factors, which can be offset by each other, every factor can be viewed as

independent (Hedayat et al., 1999). Take factor A for example. When the level of factor A increases, all other factors (B, C, D) on 4 levels appear only once on "horizontal face" in Figure 3-9.

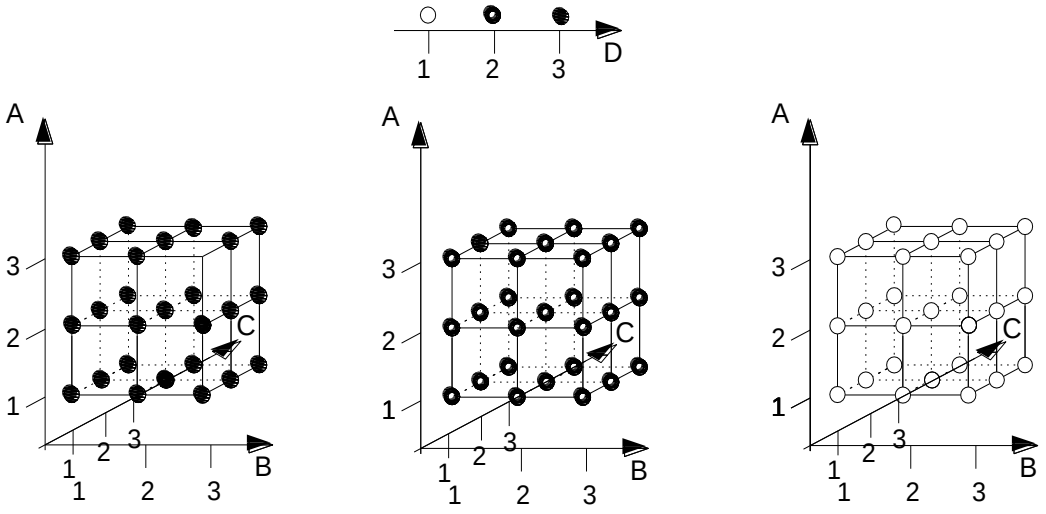

Figure 3-8 3^4 **Full Factorial Design**

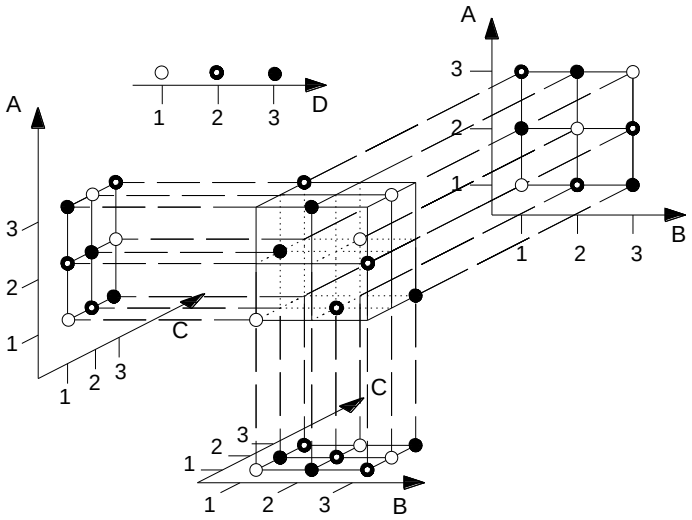

Figure 3-9 3^{4-2} **Fractional Factorial Design**

This property makes this fractional factorial design to obtain two properties: 1) no factor is redundant and unimportant (in other words, all factors are strongly representatives); 2) because all interactions are neglected, the main effect of every factor

can be observed individually. This property also makes orthogonal design to lack information about interactions and the main effects of individual factors are only general tendency, not accurate enough. So, this fractional factorial design is also termed as orthogonal main effect design.

The test arrangement in Figure 3-9 can be transferred into Table 3-7.

Table 3-7 Orthogonal Table of $L_9(3^{4-2})$

Factor / Level / Test	A	B	C	D
1	1	1	1	1
2	1	2	2	2
3	1	3	3	3
4	2	1	2	3
5	2	2	3	1
6	2	3	1	2
7	3	1	3	2
8	3	2	1	3
9	3	3	2	1

For this orthogonal array, all columns can be deemed as vectors, such as A [1,1,1,2,2,2,3,3,3], B[1,2,3,1,2,3,1,2,3], C[1,2,3,2,3,1,3,1,2], and D[1,2,3,3,1,2,2,3,1]. Mathematically, two vectors are orthogonal when their dot product is zero. Apparently, in this case, dot product by any two vectors is not zero, but equal. If the codes of three levels are replaced by -1, 0, and +1, the dot product by any two vectors will be zero. This is a good method to check whether the fractional factorial design is orthogonal.

For any fractional factorial design, the array can be expressed by the symbol as OA (N, k, s, t) (Hedayat et al., 1999). Number of tests, factors, and levels are represented by parameters N, k, and s, respectively. In this case, the orthogonal design can be described as OA (9, 4, 3, 2).

3.2.1.2 Four-level Fractional Factorial Design

The $L_{16}(4^{5-3})$ table which was obtained from Sloane's website is adjusted and used in this specific situation, with the array listed in Table 3-8. Table 3-8 shows that every 4 tests are conducted for each factor on each level. Within every 4 tests, other control variables on different levels appear equally. Taking factor C on level 3 (C3) for instance, test 3, test 8, test 9 and test 14 are conducted for this specific factor on specific level. A1 to A4, B1 to B4, D1 to D4 and E1 to E4 all appear only once in these 4 tests. Hence, the interactive effects are offset, and only the individual effects of each parameter are considered. Compared to the full factorial design, this four-level fractional factorial design can save substantial time and avoid redundancy.

Table 3-8 Orthogonal Table of $L_{16}(4^{5-3})$

	Factor				
Test	A	B	C	D	E
1	A4	B1	C1	D1	E1
2	A4	B2	C2	D2	E2
3	A4	B3	C3	D3	E3
4	A4	B4	C4	D4	E4
5	A1	B1	C2	D3	E4
6	A1	B2	C1	D4	E3
7	A1	B3	C4	D1	E2
8	A1	B4	C3	D2	E1
9	A2	B1	C3	D4	E2
10	A2	B2	C4	D3	E1
11	A2	B3	C1	D2	E4
12	A2	B4	C2	D1	E3
13	A3	B1	C4	D2	E3
14	A3	B2	C3	D1	E4
15	A3	B3	C2	D4	E1
16	A3	B4	C1	D3	E2

In the context of this study, the orthogonal table can be converted into Table 3-9, with the elements in Table 3-8 substituted by the involved parameters.

Table 3-9 Orthogonal Main Effect Design of $L_{16}(4^{5-3})$

	Element				
	BL	TL	BW	TW/BW	H
Test 1	95	40.1	64.3	0.85	14
Test 2	95	42.2	70.5	0.9	15.7
Test 3	95	44.6	75.2	0.94	17.5
Test 4	95	47.1	80.2	1	19.25
Test 5	80.2	40.1	70.5	0.94	19.25
Test 6	80.2	42.2	64.3	1	17.5
Test 7	80.2	44.6	80.2	0.85	15.7
Test 8	80.2	47.1	75.2	0.9	14
Test 9	85.3	40.1	75.2	1	15.7
Test 10	85.3	42.2	80.2	0.94	14
Test 11	85.3	44.6	64.3	0.9	19.25
Test 12	85.3	47.1	70.5	0.85	17.5
Test 13	90	40.1	80.2	0.9	17.5
Test 14	90	42.2	75.2	0.85	19.25
Test 15	90	44.6	70.5	1	14
Test 16	90	47.1	64.3	0.94	15.7

3.2.2 Full Factorial Design

Because the orthogonal design only concentrates on the main effect of each factor, the interactive effects within factors are neglected. However, it is possible that the interactive effects exist within these geometric factors in this case. Thus, a full factorial design is necessary to be conducted for seeking potential interactions. Moreover, full factorial design can simultaneously show the main effects and even multi-way interactive effects. These main effects and factorial interactions can be expressed in one full model. Take the below 2-factor full model for instance:

$$Y = \beta_0 + \beta_1 X_1 + \beta_2 X_2 + \beta_{12} X_1 X_2 + \varepsilon$$

In this full factorial model, β_{12} represents the interactive effect; $\beta_1$and β_2 respectively indicate the main effect of X_1 and X_2 (Hill and Lewicki, 2006). The researcher can use ANOVA in statistical software, such as SPSS, to analyze the main effects and interaction effects of these factors. Moreover, statistically, all "beta" coefficients, R-squared, t value can be obtained and then used to check some conclusions. For example, if t value of X_1 X_2 is larger than critical value, β_{12} means one variable does significantly influence the effect of another variable on response Y (Hill and Lewicki, 2006). Because full factorial design in this study is based on the results of fractional factorial design, the details of full factorial design are described later.

3.3 Stress Indicators Determination

Questionnaire survey and field survey show that RRPM suffers different failure modes under different scenarios. These failures happen on the various locations, such as top edges, top shell, and bottom surface of RRPM. In this study, four types of stresses, including von Mises stress, principal stress, shear stress on bottom, and normal stress on bottom, are analyzed to figure out which stress causes which specific failure mode. The results also can indirectly illustrate the relationship between the RRPM geometric characteristics and their failure modes.

3.3.1 Von Mises Stress

The most commonly used stress is von Mises stress, which is also termed as equivalent tensile stress. Von Mises stress is determined by principal stresses in three directions, as shown in the following equation:

$$2\sigma_v^2 = (\sigma_1 - \sigma_2)^2 + (\sigma_2 - \sigma_3)^2 + (\sigma_3 - \sigma_1)^2$$

where $\sigma_1, \sigma_2, \sigma_3$ are principal stresses (Wikipedia, 2012).

or expressed by normal stresses and shear stresses:

$$2\sigma_v^2 = (\sigma_{11} - \sigma_{22})^2 + (\sigma_{22} - \sigma_{33})^2 + (\sigma_{33} - \sigma_{11})^2 + 6(\sigma_{23}^2 + \sigma_{31}^2 + \sigma_{12}^2)$$

where $\sigma_{11}, \sigma_{22}, \sigma_{33}$ are normal stresses and $\sigma_{12}, \sigma_{23}, \sigma_{13}$ are shear stresses (Wikipedia, 2012).

Above equations show that the von Mises stress is a scalar stress value, which can be used to formulate the von Mises yield criterion. The von Mises yield criterion is independent of the first stress invariant, so it is "applicable for the analysis of plastic deformation for ductile materials" (Wikipedia, 2012).

3.3.2 Principal Stress

Von Mises stress only indicates the scalar stress value. To obtain the specific magnitudes and location of compressive stress and tensile stress, the principal stresses in three dimensions are calculated sequentially: maximum principal stress, middle principal stress and minimum principal stress. The signs of these principal stresses reflect whether the stress is compressive or tensile.

Normally, the damage happens on top edges and non-lens sides of marker are mainly caused by compressive stress, while the mid-bottom fracture and body bend of markers are caused more frequently by tensile stress (Zhang et al., 2009).

Depending on the distributions of these principal stress and their corresponding failure modes, it is desired to improve the RRPM geometric designs to decrease the magnitudes of these principal stresses.

3.3.3 Shear Stress on RRPM Bottom

Literature and field surveys show that, besides the abrasion and cracks of RRPM body and lens, the retention failure is another main failure mode of RRPMs. The poor

retention performance is mainly caused by shear stress, which is introduced by impact from high-speed moving vehicles. This shear stress occurs on the interface of marker and adhesive. In this study, the shear stress on the RRPM bottom face is calculated.

3.3.4 Normal Stress on RRPM Bottom

Similar to shear stress damage, the damage caused by normal stress also cripples the RRPM service life significantly, which is especially manifested as sinking into flexible surface of asphalt concrete pavement. Moreover, normal stress at RRPM bottom may cause tensile failure. Therefore, quantification of normal stress at RRPM bottom is very necessary, not only to prevent sinking, but also to avoid detachment.

CHAPTER 4: ANALYSIS OF SIMULATION RESULTS

Based on the main methodologies which are introduced in Chapter 3, the relationship between stresses, failure modes, and RRPM profiles can be connected. As reflected in Figure 4-1 to Figure 4-6, the magnitudes and locations of various stresses are shown in the snapshots of the FEM of RRPMs of different sizes. Then, these figures are compared with the images taken from field survey to deduce the relations between stress and failure modes. After constructing the connection between stresses and failure modes, statistical analysis of simulation results are made to suggest any relationship between the stresses and geometric parameters. According to the connections between stresses, failure modes, and RRPM profiles, this chapter finally provides some geometrical countermeasures for the specific failure modes.

4.1 Magnitudes and Distributions of Stresses on RRPMs

4.1.1 Von Mises Stress Magnitude and Distribution

As mentioned in section 3.3.1, von Mises stress is a scalar stress value that shows any "combined stress" distribution on the RRPMs. Figure 4-1, which is plotted by ANSYS, shows the von Mises stresses on the RRPMs of different sizes.

Figure 4-1 shows that the von Mises stress is mainly distributed on the edge of marker's top and the sides with no lens, which may cause cracks on these sides. The von Mises stress also occurs on the upper corner of lens, which probably causes the lens abrasion and crack.

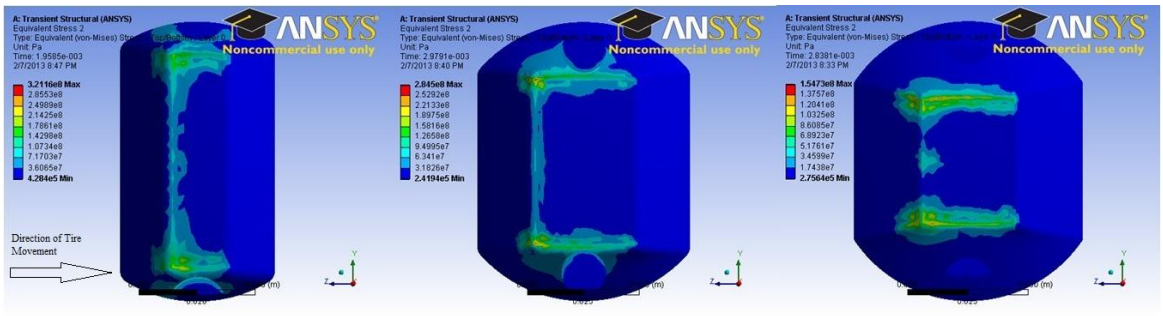

Figure 4-1 Von Mises Stress Distribution

The von Mises stress magnitude is ranging from 150MPa to 300MPa. The distribution patterns of von Mises stress do not change significantly when the RRPM size changes.

For more clearly understanding the von Mises stress distribution, the deformations of RRPM and tire are also plotted by ANSYS, shown in Figure 4-2. Figure 4-2 illustrates why von Mises stress concentrates on the no-lens sides of marker's top shell: the deformation of tire is concave-up and it makes the tire surface contact with the marker on the no-lens sides of marker's top shell.

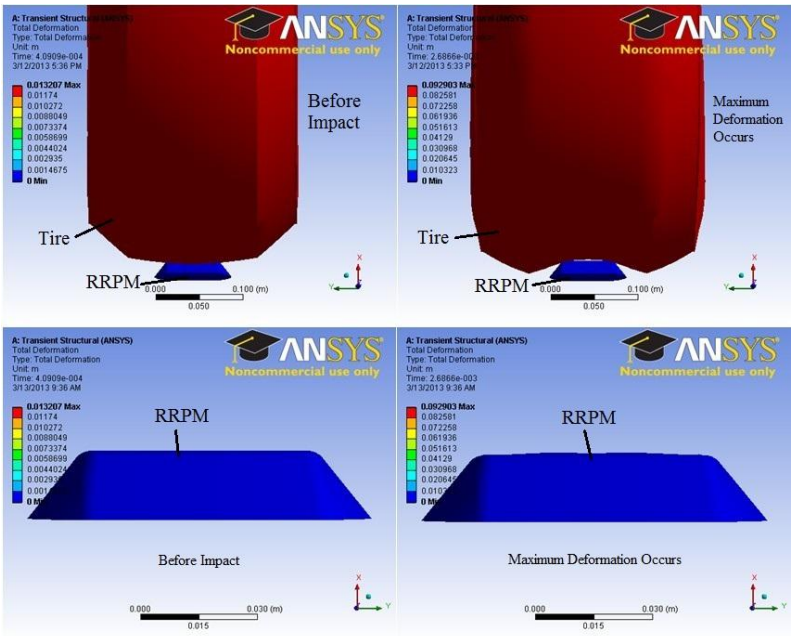

Figure 4-2 Deformations of Tire and RRPM

4.1.2 Principal Stress Magnitude and Distribution

Because von Mises stress is a scalar stress, it cannot be used to identify whether the stress condition is compressive or tensile. Thus the maximum and minimum principal stresses are required for more detailed analysis.

In ANSYS, the negative sign of principal stress indicates compressive stress and the positive sign means tensile stress. Figure 4-3 shows the maximum principal stress and Figure 4-4 shows the minimum principal stress.

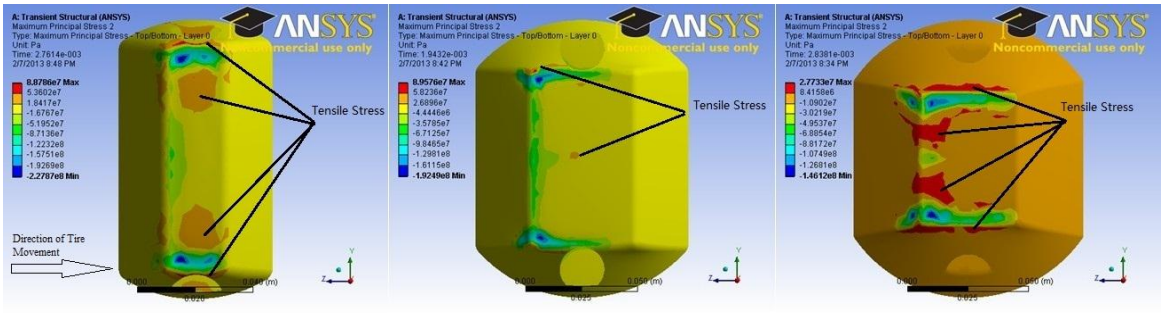

Figure 4-3 Maximum Principal Stress Distribution

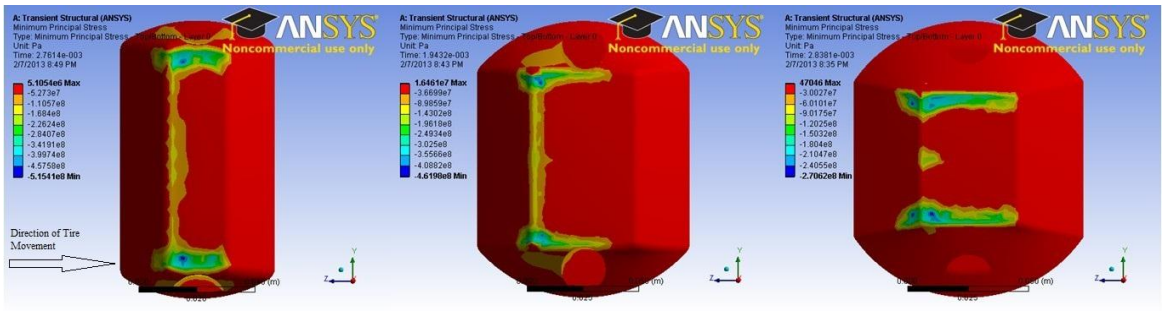

Figure 4-4 Minimum Principal Stress Distribution

Figure 4-3 and Figure 4-4 show that the magnitude of the minimum principal stress is significantly higher than that of the maximum principal stress.

Specifically, compared to the von Mises stress, the maximum tensile stress in Figure 4-3 occurs close to the middle of shell symmetrically, and also on the non-lens sides. Its distribution changes obviously when the size of marker changes.

The minimum principal stress distribution is similar to the distribution of von Mises stress. Because the magnitudes of compressive stress are noticeably larger than those of tensile stress, the lowest compressive stress and the highest tensile stress both are expressed in red color in ANSYS, and thus cannot be identified from each other clearly in Figure 4-4.

4.1.3 Shear Stress Magnitude and Distribution

Compared to the above stresses, shear stress has the most complicated magnitude and distribution, which is shown in Figure 4-5. The value of shear stress in one case probably is three times larger than that in another case. Figure 4-5 illustrates that the shear stresses having equal magnitudes symmetrically distribute on the opposite directions. The maximum shear stresses occur on the non-lens bottom sides of the RRPM, whose parts are extended by curves.

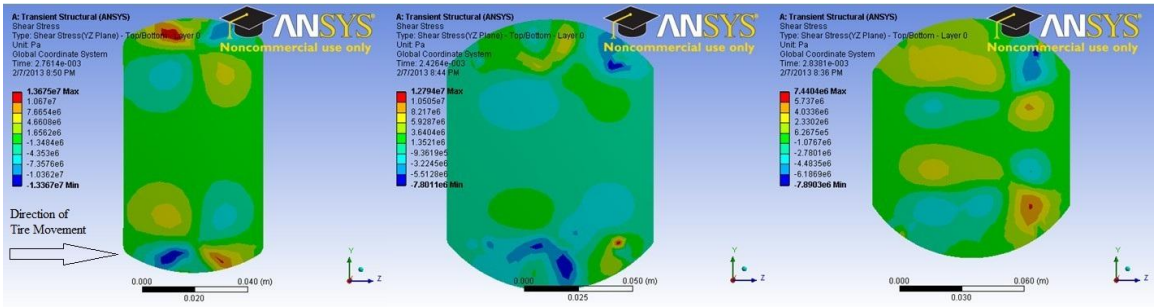

Figure 4-5 Shear Stress Distribution on Bottom of RRPM

4.1.4 Normal Stress Magnitude and Distribution

For normal stress, there is one dilemma condition: its magnitude should be neither too low, for avoiding detachment, nor too high, which can make the RRPM sink into the surface of the asphalt pavement. Its distribution is shown in Figure 4-6.

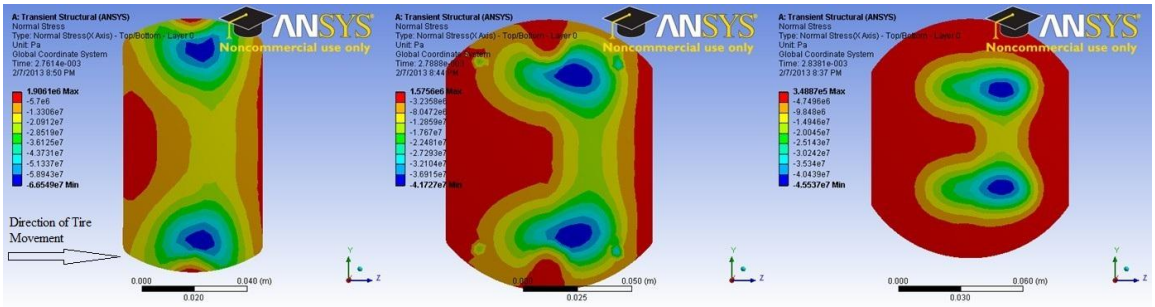

Figure 4-6 Normal Stress Distribution on Bottom of RRPM

Figure 4-6 illustrates that some upward stresses exist on the RRPM bottom. These upward normal stresses, which potentially can detach the marker from the pavement surface, are concentrated on the edges of the lens sides and the centers of the curved edges. Although the magnitude of this normal stress is not large, for the adhesive with weak tensile strength, the upward stresses may detach the RRPMs. Compared to the upward normal stress, the downward normal stress is significantly larger and distributed more regularly.

4.1.5 Relation between Stress and Failure Mode

This section summarizes the connection between the stresses and the failure modes, depending on their locations and magnitudes. The analysis of simulation results have been performed in the section 4.1.1 through 4.1.4. Table 4-1 lists the observed results. The failure modes in Table 4-1 are only potential ones, because of the limited FEM simulations and missing considerations of material strength of RRPMs. In Table 4-1, the tensile stress and compressive stress represent the maximum and minimum principal stresses, respectively. Moreover, considering the similar distributions of minimum principal stress and von Mises stress, the von Mises stress is not listed in Table 4-1.

Table 4-1 Stresses and Their Related Failure Modes

Stress Type	Potential Failure Modes
Compressive Stress	1. Cracks or breakage on the corner of the top surface of RRPM 2. Crack or abrasion on the non-lens side of the top surface of RRPM 3. Crack or abrasion on the slope of non-lens curve side
Tensile Stress	1. Crack or abrasion on the non-lens side of RRPM top 2. Crack or breakage close to middle of RRPM top shell
Shear Stress on Bottom	1. Detach the marker from pavement
Normal Stress on Bottom	1. Detach the marker from pavement 2. Sinking into asphalt

4.2 Fractional Factorial Design Results

With respect to the geometric characteristics of RRPMs, only five factors, including bottom length (BL), top length (TL), bottom width (BW), top width (TW) and height (H) are selected as candidates to investigate their roles on the mechanical response of RRPM. Due to the complexity of the process of tire-marker contact and the unclear influence of these geometric factors on RRPM, one main effect design, which is termed as orthogonal design, is necessary. As mentioned in the methodology part in Section 3.2.1, the orthogonal design is used to determine the main effects of these geometric factors. In this orthogonal design, to make sure that the bottom width is larger than the top width, a ratio of top width and bottom width is used to replace the top width.

The strain and stress conditions of RRPM in these tests are calculated by the FEM software, ANSYS. Table 4-2 shows the details of this orthogonal design and relevant results.

Each factor on each level has four tests and the average result from these four tests represents the result on that level without interactions from other factors, as shown in Table 4-3. The signs of shear stresses on bottom represent only direction and their

magnitudes are symmetrical. Therefore, for the shear stress part, Table 4-3 only lists the average value of bottom shear stress for analysis.

Table 4-2 Details of Orthogonal Design and Results of Tests

	Element (mm)					Von Mises Stress (MPa)	Maximum Principal Stress (MPa)	Minimum Principal Stress (MPa)	Normal Stress On Bottom (MPa)		Shear Stress On Bottom (MPa)	
Test	BL	TL	BW	TW/ BW	H				Max	Min	Max	Min
1	95	40.1	64.3	0.85	14	154.73	27.73	-270.62	0.59	-45.54	-7.89	7.44
2	95	42.2	70.5	0.9	15.7	178.05	50.93	-329.20	0.97	-44.78	-12.49	10.02
3	95	44.6	75.2	0.94	17.5	215.57	77.88	-359.39	1.20	-41.51	-13.20	9.88
4	95	47.1	80.2	1	19.25	284.5	90.26	-461.98	1.64	-41.73	-8.14	12.79
5	80.2	40.1	70.5	0.94	19.25	235.63	55.87	-409.47	0.06	-38.97	-9.43	9.12
6	80.2	42.2	64.3	1	17.5	239.12	63.18	-389.48	0.14	-43.06	-5.14	5.11
7	80.2	44.6	80.2	0.85	15.7	213.05	51.50	-347.48	2.45	-47.18	-12.59	11.77
8	80.2	47.1	75.2	0.9	14	183.83	30.31	-290.83	3.34	-46.74	-21.57	16.47
9	85.3	40.1	75.2	1	15.7	241.66	54.51	-361.79	0.89	-45.91	-10.39	8.99
10	85.3	42.2	80.2	0.94	14	217.5	51.86	-355.39	1.12	-51.93	-14.79	14.17
11	85.3	44.6	64.3	0.9	19.25	267.03	62.04	-358.00	0.05	-34.75	-14.25	12.50
12	85.3	47.1	70.5	0.85	17.5	231.93	56.85	-396.02	0.22	-39.75	-13.22	13.88
13	90	40.1	80.2	0.9	17.5	219.22	70.75	-348.76	1.01	-42.20	-16.27	12.16
14	90	42.2	75.2	0.85	19.25	243.7	54.21	-365.20	0.69	-37.33	-10.89	14.67
15	90	44.6	70.5	1	14	167.58	45.66	-251.84	1.02	-46.96	-13.95	8.05
16	90	47.1	64.3	0.94	15.7	188.52	46.42	-340.02	0.65	-42.37	-14.68	15.62

Table 4-3 Final Processed Results of Orthogonal Experiments (unit: MPa)

	Von Mises stress				
lv.	BL	TL	BW	TW/BW	H
1	208.2125	212.81	212.35	210.8525	180.91
2	217.9075	219.5925	203.2975	212.0325	205.32
3	239.53	215.8075	221.19	214.305	226.46
4	204.755	222.195	233.5675	233.215	257.715
	Maximum Principal Stress				
lv.	BL	TL	BW	TW/BW	H
1	50.2145	52.216	49.843	47.572	38.88925
2	56.3145	55.04225	52.323	53.50625	50.84075
3	54.25825	59.269	54.22625	58.00625	67.16275
4	61.6985	55.9585	66.0935	63.40125	65.593

Table 4-3 Continued

	Minimum Principal Stress				
lv.	BL	TL	BW	TW/BW	H
1	-359.315	-347.66	-339.53	-344.83	-292.17
2	-367.8	-359.8175	-346.6325	-331.6975	-344.6225
3	-326.455	-329.1775	-344.3025	-366.0675	-373.4125
4	-355.2975	-372.2125	-378.4025	-366.2725	-398.6625
	Normal Stress (Minimum)				
lv.	BL	TL	BW	TW/BW	H
1	1.496979	0.635099	0.353364	0.98702	1.516865
2	0.568482	0.726103	0.565426	1.339509	1.23524
3	0.839828	1.176887	1.529635	0.755776	0.64089
4	1.095263	1.462463	1.552125	0.918245	0.607555
	Normal Stress (Maximum)				
lv.	BL	TL	BW	TW/BW	H
1	1.496979	-43.155	-41.431	-42.448	-47.7905
2	0.568482	-44.2735	-42.6163	-42.117	-45.0618
3	0.839828	-42.602	-42.8693	-43.6943	-41.628
4	1.095263	-42.6448	-45.7588	-44.416	-38.195
	Average Shear Stress on Bottom				
lv.	BL	TL	BW	TW/BW	H
1	11.3986	10.21018	10.3274	11.54409	13.04086
2	12.77293	10.90919	11.26919	14.465	12.0688
3	13.28565	12.02495	13.25735	12.61046	11.10611
4	10.23286	14.54573	12.8361	9.070488	11.47426

The gray areas in Table 4-3 indicate that the factors have consistent impact on the related stress in RRPMs. Specifically, height is the dominating factor that influences the von Mises stress, minimum principal stress, normal stress and one direction shear stress on the bottom surface of RRPM; ratio of bottom width to top width influences the von Mises stress, and both principal stresses in the RRPM body; Bottom width also can individually influence the maximum principal stress, bottom normal stress and o shear stresses; Top length is independent of normal stress and shear stress on the bottom surface of RRPM; Bottom length has no main effect on any type of stress.

These consistency relations are also shown in Figure 4-7 through Figure 4-12. The impacts of each factor are plotted to suggest the developing trends. It is worth pointing out that, although the average shear stress at the bottom surface has no consistent trends in terms of bottom width and height, the negative shear stress at the bottom surface is significantly influenced by the bottom width and the positive one has consistent relationship with height. In this case, these three factors (TL, BW and H) are all found to significantly influence the shear stress on RRPM bottom. Moreover, because the sign of minimum principal stress only represents stress direction, for better observation of magnitude trend, its negative sign is converted into positive one in Figure 4-9.

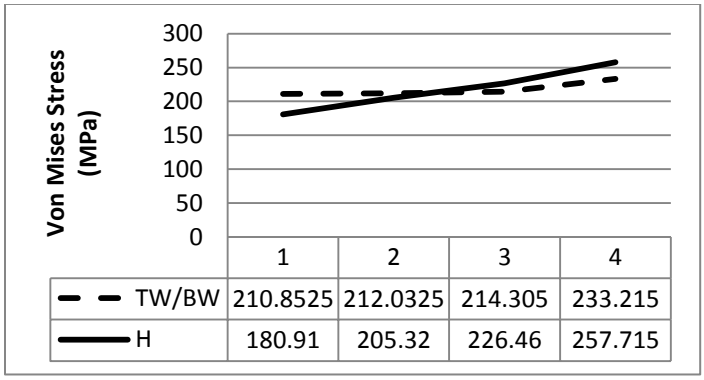

Figure 4-7 Von Mises Stress vs. Height and Ratio of Top Width and Bottom Width

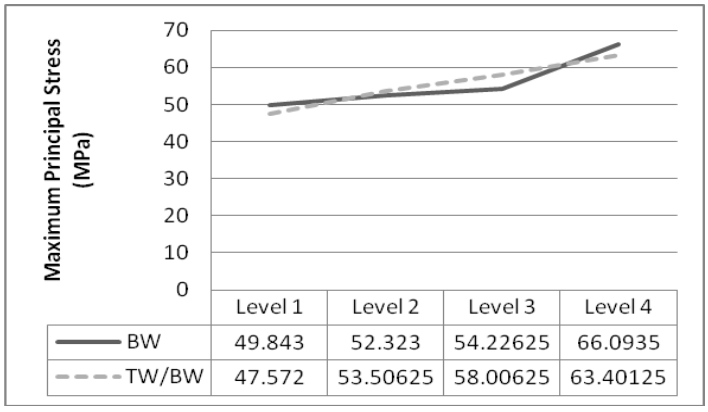

Figure 4-8 Maximum Principal Stress vs. Bottom Width and Ratio of Top Width and Bottom Width

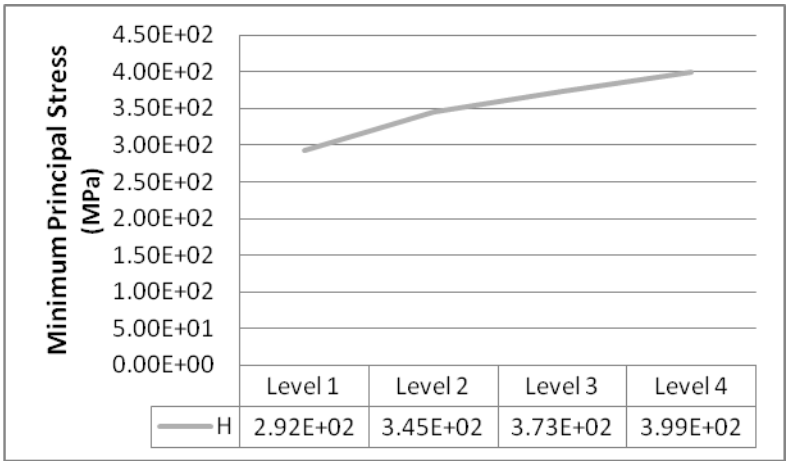

Figure 4-9 Minimum Principal Stress vs. Height

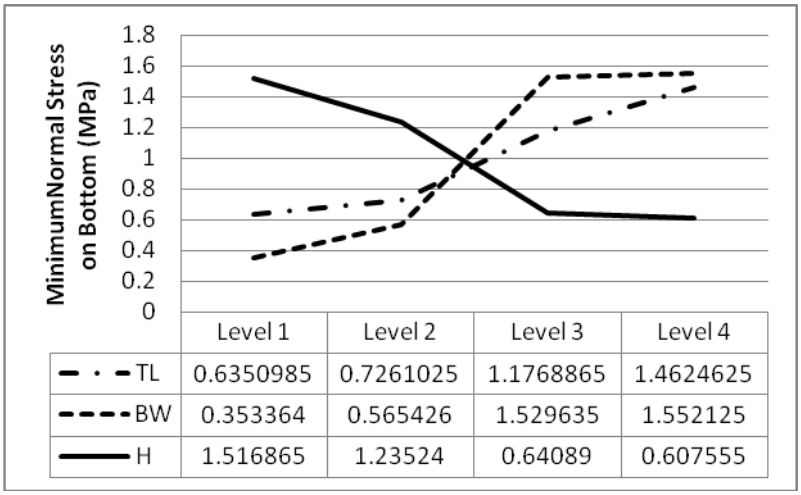

Figure 4-10 Minimum Normal Stress vs. Height, Top Length, and Bottom Width

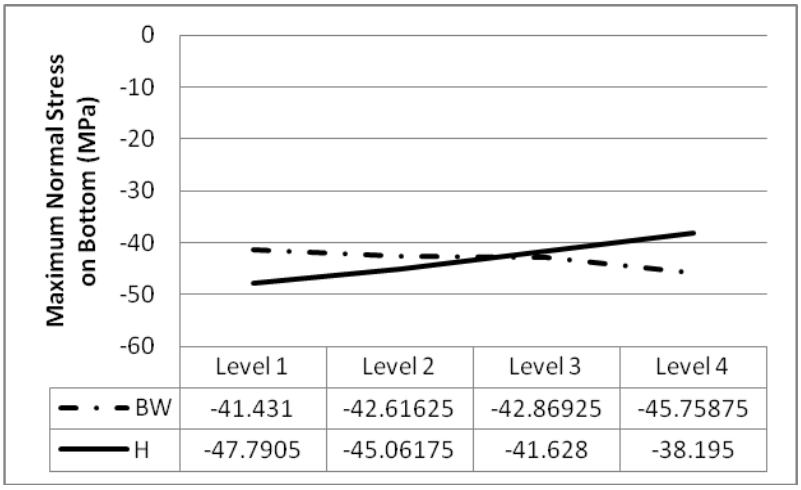

Figure 4-11 Maximum Normal Stress vs. Bottom Width and Height

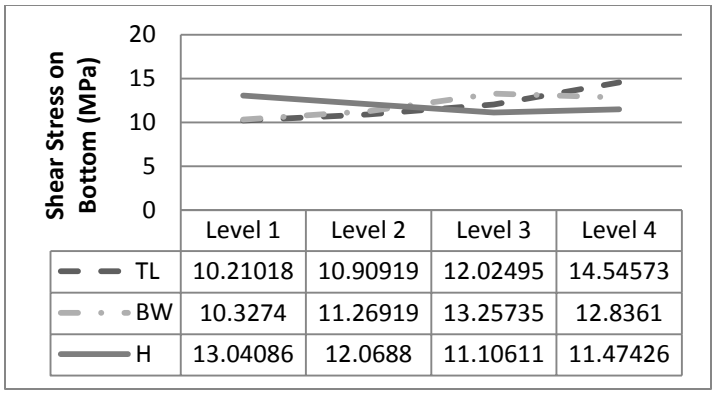

Figure 4-12 Shear Stress vs. Bottom Width, Top Length and Height

The results from Figure 4-7 through Figure 4-12 are listed in Table 4-4. In this table, "+" means positive relation and "–" stands for negative relation. Table 4-4 shows that decreasing height can reduce von Mises stress and minimum principal stress in RRPM body. However, decreasing height also causes the increase of normal stress and shear stress on RRPM bottom. The enlarged bottom width makes maximum principal stress, normal stress and shear stress increase. The same relation is found between top length, with minimum normal stress and shear stress. Moreover, the less the ratio of top width and bottom width is, the less the von Mises stress and maximum principal stress are.

Table 4-4 Trends of Stress Magnitudes in Terms of Geometric Factors

	Stress					
Geometric Factor	Equivalent Stress	Maximum Principal Stress	Minimum Principal Stress	Maximum Normal Stress	Minimum Normal Stress	Shear Stress
Height	+		+	-	-	-
Ratio of Top Width and Bottom Width	+	+				
Bottom Width		+		+	+	+
Top Length					+	+
Bottom Length						

4.3 Full Factorial Design Results

The results of orthogonal design illustrates that the bottom length has no consistent influence on stresses. However, it is also possible that the length and width have some interactions, which cause the inconsistent results from orthogonal design. To check these main effects and possible existing interactions of the two geometric factors, a 4×5 full factorial design was conducted. In this full factorial design, height, the slope of lens, the ratio of bottom width and top width are constant. Two factors, length and width, are defined respectively at four and five levels, as shown in Table 4-5.

Table 4-5 Full Factorial Design

Tests No.	BL	TL	BW	H	TW
1	53.13	21.83	80.2	17.5	80.2
2	64.515	33.215	80.2	17.5	80.2
3	75.9	44.6	80.2	17.5	80.2
4	87.285	55.985	80.2	17.5	80.2
5	53.13	21.83	75.2	17.5	75.2
6	64.515	33.215	75.2	17.5	75.2
7	75.9	44.6	75.2	17.5	75.2
8	87.285	55.985	75.2	17.5	75.2
9	53.13	21.83	70.2	17.5	70.2
10	64.515	33.215	70.2	17.5	70.2
11	75.9	44.6	70.2	17.5	70.2
12	87.285	55.985	70.2	17.5	70.2
13	53.13	21.83	65.2	17.5	65.2
14	64.515	33.215	65.2	17.5	65.2
15	75.9	44.6	65.2	17.5	65.2
16	87.285	55.985	65.2	17.5	65.2
17	53.13	21.83	60.2	17.5	60.2
18	64.515	33.215	60.2	17.5	60.2
19	75.9	44.6	60.2	17.5	60.2
20	87.285	55.985	60.2	17.5	60.2

The stress conditions of RRPM in these tests are also calculated using the FEM software, ANSYS. The simulation results and variables can be fed into SPSS program to

analyze the interactive effects by building regression model. Because the changes of top length and top width are identical to those of bottom length and bottom width, only bottom length and bottom width are considered in the regression model.

The results obtained from the full factorial design can be used in two different regression models. One is termed as two-factor interaction model for getting interactive relationships between variables. The other is named as simple additive model, which is used to check main effects of variables if the interaction is insignificant.

4.3.1 Two-Factor Interaction Model

A linear regression model as shown below is used for data analysis. In this model, BL*BW represents the interaction between bottom length and bottom width.

$$ES = \beta_0 + \beta_1 BL + \beta_2 BW + \beta_3 BL \cdot BW + \varepsilon$$

The adjusted R squared, coefficient of each variable, and t-value can be calculated by SPSS program to check whether there are statistically significant impacts of interactions between length and width on the specific stresses.

Table 4-6 Statistical Analysis Results of Two Factor Interaction Model by SPSS

Model 1							
	Adjusted R Squared	df	F	Coefficients			
				Variables	Standardized Coefficients	t	Sig.
Equivalent	0.382	3	4.92	BL	1.184	0.658	0.52
Stress		16		BL*BW	-1.986	-0.966	0.348
		19		BW	1.351	1.336	0.2
Maximum	0.314	3	3.898	BL	1.841	0.971	0.346
Principal		16		BL*BW	-2.758	-1.273	0.221
Stress		19		BW	1.555	1.46	0.164
Minimum	0.371	3	4.73	BL	3.187	1.755	0.098
Principal		16		BL*BW	-4.169	-2.009	0.062
Stress		19		BW	2.392	2.344	0.032

Table 4-6 Continued

Maximum	0.323	3	4.017	BL	2.531	1.343	0.198
Normal		16		BL*BW	-2.481	-1.153	0.266
Stress		19		BW	1.695	1.602	0.129
Minimum	0.858	3	39.121	BL	0.261	0.302	0.766
Normal		16		BL*BW	-1.19	-1.206	0.246
Stress		19		BW	1.094	2.253	0.039
Average	0.571	3	9.43	BL	-0.616	-0.411	0.687
Shear		16		BL*BW	1.217	0.71	0.488
Stress		19		BW	0.068	0.081	0.937

The gray area in Table 4-6 shows that the significant interaction only exists between width and length on minimum principal stress. The signal of this interactive factor is negative, which means increasing width can decrease the effect of length on minimum principal stress. On the contrary, enlarging length causes the reductions of the effect of width on minimum principal stress. One concept should be pointed out is that, although the interactive effect is the multiplicative relation between width and length, it does not represent the bottom or top area.

4.3.2 Simple Additive Model

After checking interactions between width and length, a simpler model, namely simple additive model, is built to check the main effects of width and length in some scenarios without interactions.

$$ES = \beta_0 + \beta_1 BL + \beta_2 BW + \varepsilon$$

The statistical analysis results, obtained using SPSS, are shown as Table 4-7.

Table 4-7 shows that enlarging length makes von Mises stress, maximum principal stress, and minimum normal stress to decrease. It also causes the increase of

shear stress. Table 4-7 also indicates that a smaller width can reduce von Mises stress, both normal stresses, and shear stress.

Table 4-7 Statistical Analysis Results of Simple Additive Model by SPSS

Model 2							
	Adjusted R Squared	df	F	Coefficients			
				Variables	Standardized Coefficients	t	Sig.
Von Mises Stress	0.385	2	6.941	BL	-0.545	-3.031	0.008
		17		BW	0.39	2.167	0.045
		19					
Maximum Principal Stress	0.288	2	4.852	BL	-0.561	-2.9	0.01
		17		BW	0.22	1.137	0.271
		19					
Maximum Normal Stress	0.31	2	5.26	BL	0.371	1.944	0.069
		17		BW	0.495	2.597	0.019
		19					
Minimum Normal Stress	0.854	2	56.449	BL	-0.775	-8.836	0
		17		BW	0.518	5.902	0
		19					
Average Shear Stress	0.584	2	14.309	BL	0.443	2.993	0.008
		17		BW	0.656	4.434	0
		19					

The results obtained by full factorial experiment are shown in Table 4-8, which is described in the same format of Table 4-4.

Table 4-8 Tendency of Stress Magnitudes with Bottom Width and Length

	Stress					
Geometric Factor	Equivalent Stress	Maximum Principal Stress	Minimum Principal Stress	Maximum Normal Stress	Minimum Normal Stress	Shear Stress
Width	+	+		+	+	+
Length	-	-			-	+
Interaction			-			

4.4 Relations between RRPM Profile, Stress, and Failure Mode

Section 4.1.5 shows the relationship between stress and failure mode, and Section 4.2 discusses connection between stress and RRPM profile. This section combines the former two sections together and suggests some measures to mitigate failure potentials of RRPMs.

Table 4-9 RRPM Failure Location and Possible Geometric Improvement

Location of potential failure mode	Stress	Possible countermeasure
1. On the corner of RRPM top shell	Compressive stress	Reduce height
	Von Mises stress	Reduce height, or make top width much shorter than bottom width, or shorten bottom width, or extend bottom length.
2. On the non-lens side of RRPM top shell	Compressive stress	Reduce height
	Von Mises stress	Reduce height, or make top width much shorter than bottom width, or shorten width, or extend length.
	Tensile stress	Makes top width much shorter than bottom width, or shorten width, or enlarge length, or shorten only bottom width
3. Closed to middle of RRPM top shell	Tensile stress	Makes top width much shorter than bottom width, or shorten width, or enlarge length, or shorten only bottom width
4. On the slope of non-lens curve side	Compressive stress	Reduce height
	Von Mises stress	Reduce height, or make top width much shorter than bottom width, or shorten width, or extend length.
5. RRPM bottom (detach the marker from pavement)	Shear stress	Increase height, or shorten width, or shorten length, or shorten only bottom width, or shorten only top length
	Normal stress	Increase height, or shorten width, or extend length, or shorten only bottom width, or shorten only top length
6. RRPM bottom (sinking into asphalt)	Normal stress	Increase height, or shorten width, or shorten only bottom width

In Table 4-9, the compressive stress and tensile stress represent the minimum principal stress and maximum principal stress, respectively. It is worth pointing out that, for the issue of sinking, the elastic and plastic properties of pavement are not considered.

Thus, the possible countermeasures for mitigating sinking in Table 4-9 just serve as references.

4.5 Validation by Survey Results

Section 4.1 to Section 4.3 indicate that, typically, shorter bottom width and top length, longer bottom length, lower height, and lower ratio of top width over bottom width can mitigate RRPM body damages. However, for the sinking and detachment on RRPM bottom, the lower RRPM height and the longer RRPM length may deteriorate both of these failure modes.

Chapter 2 already lists the estimated rank of RRPMs in Florida as: 3M 290> Rayolite RS >Ennis 980>Ennis C80>Apex 921AR. Their geometric characteristics are shown as follows.

Table 4-10 Geometric Characteristics of RRPM Types

Type	Height	Bottom Length	Bottom Width	Top Length	Top Width	Ratio of Top Width over Bottom Width
3M 290	15.7	88.9	72.3	44.9	69.8	0.97
Ennis C80/980	17.5	80.8	86.3	39.2	78	0.9
Apex 921AR	18.1	101	101	40.1	85.8	0.85
Rayolite RS	17.3	99.3	100.2	48.8	57.5	0.57

On the perspective of body damage, Table 4-10 illustrates that 3M 290 has two best designed geometric factors, and each of other three types individually has one best profile factor. Moreover, for Rayolite RS, although its bottom width is widest and its height is highest, its extreme lowest ratio of top width over bottom width makes this RRPM type retain excellent performance. This phenomenon is validated by the results of surveys: 3M 290 is best, and Rayolite RS is slightly better than the rest.

For failure mode, field survey shows that the middle of 3M 290 top shell seems much weaker than the other types of RRPMs. It can also be explained by Table 4-9 and Table 4-10: the highest ratio of top width and bottom width and the low bottom length both can produce high tensile stress, and then induce cracks in the middle of RRPM shell. Moreover, because the height of 3M 290 is lowest, the detachment and sinking occur more probably.

For Rayolite RS, its high height, high bottom width and top length also generate high compressive stress around its top corner and non-lens sides, and cause cracks more probably. The lowest ratio of top width and bottom width prevents Rayolite RS from cracking on the middle of its top shell.

CHAPTER 5: CONCLUSIONS AND FUTURE RESEARCH

5.1 Conclusions

This research conducts literature review, field surveys and questionnaire surveys of various types of RRPMs and compares their current performances. The rank of the RRPM performances in Florida is as: 3M 290> Rayolite RS >Ennis 980>Ennis C80>Apex 921AR. This rank is used to validate the simulation results from FEMs.

Based on the tire/marker/pavement FEM system built in ANSYS, the general distributions and magnitudes of stresses are observed and obtained. The von Mises stress and compressive stress are mainly distributed on the edge and corner of marker's top and the sides with no lens. The main tensile stress is near the middle of shell and symmetrically distributed. Moreover, the magnitude of tensile stress is much less than that of the compressive stress. For shear stress, maximum one occurs on the non-lens bottom sides of the RRPM, which are extended by curves. Compared to other stresses, shear stress distributes at RRPM bottom with more irregularity, but symmetrically. The upward normal stress also exists at the bottom, and is mainly concentrated on the edge of lens side and in the middle of the curve edge.

To obtain the relationship between stress and RRPM profile, one $\mathbf{L}_{16}(4^{5-3})$ orthogonal design and one 4×5 full factorial design with a statistical significance level of 10% are conducted. The findings are summarized as follows.

1) Decreasing height can reduce von Mises stress and minimum principal stress on RRPM body. However, decreasing height also leads to the increase of normal stress and shear stress at RRPM bottom.

2) For the profile of RRPM bottom surface, the enlarged bottom width causes tensile stress (on RRPM body), normal stress and shear stress (at RRPM bottom) to increase. Only changing bottom length cannot determine the stress developing tendency.

3) For the shape of RRPM top shell, increasing top length has no significant influence on most stresses, except for increments of the tensile stress and shear stress at RRPM bottom.

4) The less ratio of top width and bottom width can mitigate the von Mises stress and tensile stress on RRPM body.

5) The significant interactive effect between bottom width and length exists on minimum principal stress, with the significance level of 10%. This interactive effect means increasing bottom width can decrease the effect of bottom length on minimum principal stress.

6) Keeping the RRPM height, the slope of lens, the ratio of bottom width and top width as constants, the RRPM width has positive and significant influence on von Mises stress, tensile stress on RRPM body, and normal stresses and shear stress at RRPM bottom. On the contrary, the RRPM length affects von Mises stress, tensile stress (on RRPM body), and compressive stress (at RRPM bottom) negatively and significantly. However, shortening RRPM length can efficiently mitigate the detachment failure mode through decreasing shear stress (at RRPM bottom).

According to the relationship between stress location, potential failure mode, and RRPM profile, some possible countermeasures are suggested and listed in Table 4-9 to improve the geometric designs of RRPMs. Specifically, for Rayolite RS, its low ratio of top width and bottom width strengthens the middle of RRPM top shell significantly. However, if Rayolite RS can decrease its bottom width and top length, the cracks which are produced frequently on the rims can be prevented efficiently. For 3M 290, although its height and bottom width are more optimal than those of other RRPM types, the cracks often occur on the middle of RRPM shell. For mitigating this type of structural damage, 3M 290 can shorten its top width.

5.2 Future Research

The full factorial experiment in this thesis is only about two factors. The improved full factorial experiment shall be conducted. The RRPM height, top width and length need to be considered in the improved full factorial experiment.

The RRPM model in this thesis is simple, without any fillet and chamfer. These RRPM geometric characteristics can also be considered for affecting stress conditions.

REFERENCES

ANSYS. (2009). *Contact Technology Guide*. ANSYS, lnc, Canonsburg, PA.

ASTM. (2001). *Standard E 1845-01Standard Practice for Calculating Pavement Macrotexture Mean Profile Depth*. ASTM, International, West Conshohocken, PA.

ASTM. (2006). *Standard E 274-06 Standard Test Method for Skid Resistance of Paved Surfaces Using a Full-Scale Tire*. ASTM International, West Conshohocken, PA.

ASTM. (2008). *Standard Specification for Extended Life Type, Nonplowable, Raised Retroreflective Pavement Markers*. ASTM International, West Conshohocken, PA, pp. 1-9.

FDOT. (2010). *FDOT Design Standards: Typical Placement of Reflective Pavement Markers.* Florida Department of Transportation, pp. 1-2.

FDOT. (2012). *Qualified Product List S706.* Florida Department of Transportation, pp.1.

FHWA. (2003). *Manual on Uniform Traffic Control Devices for Streets and Highways.* Federal Highway Administration, U.S. Department of Transportation, http://mutcd.fhwa.dot.gov/htm/2003r1/part3/part3b1.htm Accessed August 10, 2012.

Hedayat, A.S., Sloane, N.J.A., and Stufken, J. (1999). *Orthogonal Arrays*: *Theory and Applications*, New York: Springer.

Hill, T., and Lewicki, P. (2006). *Statistics: Methods and Applications*. StatSoft, ISBN 1-884233-59-7.

Hofmann, K.L., and Dunning, M. (1995). *Evaluation of Raised and Recessed Pavement Markers Final Report.* Oregon Department of Transportation. OD-RD-96-06, pp.3.

Kosgolla, J.V. (2012). *Numerical Simulation of Sliding Friction and Wet Traction Force on A Smooth Tire Sliding on A Random Rough Pavement*, dissertation work, Civil and Environmental Engineering, University of South Florida.

Matthias, J.S. (1988). *Spacing of Raised Reflective Pavement Markers.* Arizona Department of Transportation, FHWA-AZ88-836.

NCHRP. (2004). *Safety Evaluation of Permanent Raised Pavement Markers.* National Cooperative Highway Research Program, Report 518, Project G5-17 FY'01.

NTPEP. (2004). *Laboratory and Field Evaluations of Bituminous Pavement Marker Adhesive Georgia Test Deck Two Year Evaluation*. National Transportation Product Evaluation Program, pp. 20-22.

NTPEP. (2011). *Laboratory and Field Evaluations of Permanent Non-plowable Raised Pavement Markers Georgia Test Deck Two Year Evaluation*. National Transportation Product Evaluation Program, pp. 43-44.

Wikipedia. (2013). *Von Mises Yield Criterion.* The free encyclopedia. http://en.wikipedia.org/wiki/Von_Mises_yield_criterion , accessed on January 27, 2013.

Zador, P.L., Wright, P.H., and Karpf, R.S. (1982). *Effect of Pavement Markers On Nighttime Crashes in Geogia.* Insurance Institute for Highway Safety.

Zhang, Y., Tong, J., Carlson, P., Hawkins, G., and Keating P. (2009). *Development of measures to improve field performance of retroreflective raised pavement markers.* Texas Transportation Institute. Project 0-5089, Technical Report 0-5089-1, pp.1, 130.